Reconstructing paleoenvironments of the Late Cretaceous Western Interior Seaway, USA, using paired triple oxygen and carbonate clumped isotope measurements

Jordan A.G. Wostbrock[1], James D. Witts[2,3], Yang Gao[4], Catherine Peshek[3], Corinne E. Myers[3], Gregory Henkes[4], and Zachary D. Sharp[3]

[1]Yale University, Earth and Planetary Sciences, 210 Whitney Ave, New Haven, CT, 06511

[2] The Natural History Museum, Cromwell Road, London, UK, SW7 5BD

[3]University of New Mexico, Earth and Planetary Sciences, Northrop Hall, Albuquerque, NM, 87131

[4]Stony Brook University, Department of Geosciences, 255 Earth and Space Building, Stony Brook, NY, 11794

ABSTRACT

Fossiliferous carbonate concretions are commonly found in sediments deposited in the Late Cretaceous Western Interior Seaway (WIS). Although concretions are diagenetic features, well-preserved fossils from within them have been instrumental in reconstructing the temperature and $\delta^{18}O$ value of WIS seawater, essential for accurate reconstruction of Late Cretaceous climate. Here, we constrain formation conditions of late Campanian and early Maastrichtian carbonate concretions by combining triple oxygen isotope measurements with carbonate clumped isotope paleothermometry on different carbonate phases within the concretions. We measured both fossil skeletal aragonite and sparry calcite infill from cracks and from within macrofossil voids to evaluate differences between 'primary' and 'altered'

geochemical signals. Based on the two temperature sensitive isotope systems of the primary fossil shell aragonite, the temperature of the WIS was between 20 and 40°C and was likely thermally stratified during the Campanian. The reconstructed $\delta^{18}O_{seawater}$ values of ~-1‰ for Campanian WIS waters are similar to those expected for the open ocean during greenhouse climates, while the Maastrichtian WIS may have been more restricted, with a $\delta^{18}O_{seawater}$ value of ~2‰, reflecting more evaporative conditions. We reconstruct the diagenetic history of the sparry infill and altered fossils using a fluid-rock mixing model. Alteration temperature, alteration fluid $\delta^{18}O$ value, and the initial formation temperature are calculated by applying the fluid-rock mixing model to a Particle Swarm Optimization Algorithm. We find a different range of initial formation temperatures between the Campanian (25-38°C) and Maastrichtian (9-28°C). We also find that alteration in the presence of light meteoric fluids ($\delta^{18}O \approx$ -10‰) are required to explain both the sparry infill and the altered fossil isotopic values. Based on our results, both lithification and alteration of the carbonates occurred soon after burial, and light meteoric fluids support prior findings that high topographic relief existed on the western margin of the WIS during the Late Cretaceous. As one of the first studies to apply these techniques in concert and across multiple mineralogical phases within samples, our results provide important constraints on paleoenvironmental conditions in an enigmatic ocean system and will improve interpretations of the overall health of ecosystems leading into the end-Cretaceous mass extinction.

INTRODUCTION

Atmospheric CO_2 levels during the Early Cretaceous were 4-7 times higher than modern, resulting in a generally warmer, greenhouse climate (Arthur et al., 1985; Royer et al., 2001; Tierney et al., 2020) and a reduced global latitudinal temperature gradient (Hay, 2008; O'Brien et al., 2017). The climate during the late Campanian and Maastrichtian stages of the Late

Cretaceous reflects a general cooling trend (Barrera and Savin, 1999; Clarke and Jenkyns, 1999; Huber et al., 1995; Huber et al., 2002; Tierney et al., 2020), and associated strengthening of global latitudinal temperature gradients (O'Brien et al., 2017) prior to the mass extinction at the Cretaceous-Paleogene boundary. In North America, fossiliferous sediments deposited in the shallow epicontinental Western Interior Seaway (WIS) contain a spectacular record of life and environments during this time period (Kauffman and Caldwell, 1993; Roberts and Kirschbaum, 1995). Nevertheless, reconstructions of oceanographic and climate conditions remain a challenge to accurately reconstruct, even though this information provides important constraints on the vulnerability of marine and terrestrial ecosystems leading into a major biotic transition (Brusatte et al., 2015; Condamine et al., 2021; Landman et al., 2015; Sakamoto et al., 2016; Stinnesbeck et al., 2012; Wang and Dodson, 2006).

The WIS underwent a regression in the Late Cretaceous following global sea level trends and uplift along its western margin, with offshore depths shallowing to <100 m (Gill and Cobban, 1966), compared to 300 m during the mid-Cretaceous highstand (Miall et al., 2008). Over this period, the connectedness of the WIS with the open ocean to the north and south is debated (Hay et al., 1993; Kauffman, 1984; Kauffman and Caldwell, 1993; Kennedy et al., 1998; Petersen et al., 2016), which is an important consideration when trying to estimate oceanographic conditions in the seaway and regional climate reconstruction in general. Kauffman (1984) and Hay et al. (1993) proposed that during the Campanian, the WIS was connected to the Gulf of Mexico, Arctic Ocean, and Hudson Bay. This open seaway would have been a well-mixed, “normal marine” water body with an oxygen isotope composition similar to the overall ocean, perhaps similar to the present-day South China Sea (Schmidt et al., 1999). Coulson et al. (2011), Kennedy et al. (1998) and others have proposed a much more restricted seaway during the

69 Campanian and subsequent Maastrichtian stage, with little connection to the north. A more
70 restricted seaway could have been isotopically distinct from the open ocean, for instance
71 featuring a higher oxygen isotope value of seawater ($\delta^{18}O_{seawater}$) due to increased evaporation,
72 similar to the present-day Mediterranean Sea (Schmidt et al., 1999). Alternatively, Petersen et al.
73 (2016) and others have proposed variable $\delta^{18}O_{seawater}$ values for the WIS due to density
74 stratification driven by large salinity gradients, similar to the present-day Chesapeake Bay (Sachs
75 and Schwab, 2011). Density stratification could have been caused by a northern influx of
76 freshwater into the evaporation-dominated, saline, and restricted WIS from two possible
77 precipitation sources: (1) high elevation runoff from the western mountain range (where $\delta^{18}O$
78 value for precipitation is estimated to be as low as -20‰ (Fricke et al., 2010) and (2) mid- to
79 low-elevation basinal precipitation (with $\delta^{18}O$ values of about -9.5 ‰ (Poulsen et al., 2007)).
80 Previous studies of WIS skeletal biogenic carbonates have mostly used $\delta^{18}O$
81 measurements to reconstruct paleotemperatures (Cochran et al., 2003; He et al., 2005; Landman
82 et al., 2018a; Rowe et al., 2020; Tourtelot and Rye, 1969; Witts et al., 2020; Wright, 1987).
83 However, the calculation to reconstruct temperature requires an assumed $\delta^{18}O_{seawater}$ value in
84 which the carbonate formed. For most of these studies, an assumption has been that WIS waters
85 were isotopically similar to the open ocean, which under ice-free Cretaceous 'greenhouse'
86 conditions, would have an average $\delta^{18}O_{seawater}$ value of -1‰ (Shackleton and Kennett, 1975).
87 However, this $\delta^{18}O_{seawater}$ value may not be an appropriate assumption for an epeiric seaway such
88 as the Late Cretaceous WIS due to the oceanographic and tectonic uncertainties detailed above.
89 Several recent studies used carbonate clumped isotopes (denoted by the isotope ratio Δ_{47}) to
90 reconstruct paleotemperature and $\delta^{18}O_{seawater}$ values of the WIS through the Late Cretaceous
91 (Dennis et al., 2013; Gao et al., 2021; Jones et al., 2022; Petersen et al., 2016; Tobin et al., 2014).

92 Carbonate Δ_{47} values are a measure of the ^{13}C and ^{18}O 'clumping' in carbonate C-O bonds,
93 which is temperature dependent and yield paleotemperatures that are independent of mineral and
94 precipitating fluid $\delta^{18}O$ values. This allows for an independent estimation of both temperature
95 and the $\delta^{18}O$ value of the water from carbonate Δ_{47} and $\delta^{18}O$ (Eiler, 2011; Huntington and
96 Petersen, 2023). However, like carbonate $\delta^{18}O$, Δ_{47} is susceptible to resetting during diagenesis
97 and is also affected by so-called 'solid state bond reordering' at elevated temperatures, which a
98 fossil shell may experience during deep to moderate sedimentary burial (Dennis and Schrag,
99 2010; Hemingway and Henkes, 2021; Henkes et al., 2014; Looser et al., 2023; Passey and
100 Henkes, 2012; Ryb and Eiler, 2018; Shenton et al., 2015; Stolper et al., 2018). Although
101 screening tests for diagenetic alteration are used to identify the most pristine fossil samples in
102 these studies (e.g., Cochran et al., 2010), a recent paper using carbonate triple oxygen isotopes
103 (paired $\delta^{17}O$-$\delta^{18}O$ analyses, reported as $\Delta'^{17}O$ values) of fossil shells demonstrated diagenetic
104 alteration of samples previously assumed to be pristine based on luminescence, microstructure,
105 and elemental (Sr, Fe, Mn) compositions (Wostbrock et al., 2020a). The triple oxygen isotope
106 values are particularly sensitive indicators of diagenesis because both $\delta^{17}O$ and $\delta^{18}O$ values have
107 identical diagenetic susceptibility (in contrast to a different potential for carbonate $\delta^{13}C$ because
108 of varying dissolved inorganic carbon concentrations in fluids; Banner & Hanson, 1999). There
109 is a unique paired equilibrium $\delta^{17}O$-$\delta^{18}O$ value of a carbonate for a given temperature in ocean
110 water with a given $\delta^{18}O$ value, meaning that deviations from the expected equilibrium value are
111 easily identifiable.

112 In this study, we paired $\Delta'^{17}O$ and Δ_{47} measurements along with traditional $\delta^{13}C$ and $\delta^{18}O$
113 measurements of carbonates found within nine concretions spanning the late Campanian and
114 early Maastrichtian in the WIS. Multiple phases and mineralogies of carbonate occur in these

concretions. Phases include crack-filling sparry calcite, void-filling sparry calcite, aragonitic fossil shells of ammonoid cephalopods and both aragonitic and calcitic fossil shells of bivalve mollusks. By targeting multiple phases within a single concretion, we further demonstrate that it is possible to "see-through" diagenesis and constrain the initial precipitation temperature of the biogenic carbonates (Wostbrock et al., 2020a; Wostbrock and Sharp, 2021). By measuring both $\Delta'^{17}O$ and Δ_{47}, we can better control for the effects of diagenesis and calculate paleotemperatures and $\delta^{18}O_{seawater}$ of the WIS using both pristine samples and altered samples; additional application of fluid-rock mixing models help to constrain the initial carbonate formation conditions in altered samples. These results are significant because they both enable the identification of diagenetic effects on common geochemical proxies used to characterize paleoenvironments and provide insight into conditions in one of the most well-studied geologic basins leading into one of the largest environmental perturbations of the Phanerozoic.

METHODS

Sample selection and formation information

Samples of fossiliferous concretions were selected for isotopic analysis to represent a variety of contemporaneous or near contemporaneous oceanographic settings such as near shore versus offshore and near methane seep versus non-methane seep (Table 1). Concretions from the Western Interior Seaway are often fossil-rich and are commonly found in continuous layers within friable shales (Reeside and Cobban, 1960; Waage, 1964). In some cases, these layers may represent subtle flooding surfaces (i.e., parasequence boundaries (Slattery et al., 2018)). They are believed to have formed during early diagenesis after rapid burial (Landman and Klofak, 2012; Maples, 1986; Zatoń and Marynowski, 2006). Maples (1986) addresses four main identifying features that indicate an early diagenetic origin: (1) the surrounding shale tends to drape over

concretions, (2) fossils are not crushed, so they must have been lithified into the concretion before further burial, (3) fossils tend to be better preserved in the concretions compared to the shale, and (4) bioturbation can be preserved in the concretions but are not observed in the host shale. Some studies suggest that concretions tend to form where clusters of mollusks were adhered or lying on the sea floor (Waage, 1964, 1968). Alternatively, shells may have accumulated preferentially in depressions on the sea floor either created biologically (e.g., depressions created from feeding rays; cf. Geraghty and Westermann, 1994), from bottom water currents (Tsujita, 1995; Zatoń and Marynowski, 2006), or a mixture of the two (Landman and Klofak, 2012). However, it is worth noting that not all concretions are fossil bearing, suggesting the presence of organic matter, not necessarily of fossils, may be necessary for concretion formation (Raiswell and Fisher, 2000, 2004).

Landman and Klofak (2012) proposed a timeline of carbonate concretion formation that occurs in 3 steps. First, over a period of less than 10 years, ammonite and other mollusk shells accumulate in localized areas due to predation and/or currents. Over the next 10–100 years the concretion forms after shallow burial with concomitant calcite formation within cracks. Finally, alteration by meteoric water during later diagenesis results in the altered fossil shell material and infilling of ammonite chambers and voids with calcite. The dissolution and reprecipitation of different carbonate phases in these concretions make them ideal samples to reconstruct the fluid that altered the materials within the concretion and calculate the pristine carbonate oxygen isotope composition. Also, the presence of discrete diagenetic phases makes for an ideal scenario to use both clumped and triple oxygen isotope geochemistry to elucidate primary versus diagenetic preservation.

For this study, concretions were collected from the Pierre Shale and Fox Hills Formations, which were deposited in the epeiric Western Interior Seaway during the Campanian and the early-mid Maastrichtian, respectively, and which today crop out in Kansas, Colorado, Wyoming, South Dakota, North Dakota, and Montana (Figure 1; Kauffman and Caldwell, 1993; Waage, 1968). These formations represent a range of offshore through deep sub-tidal to littoral depositional environments, although even in the most offshore settings, water depths in the WIS were <100 m (Gill and Cobban, 1966). The fossiliferous nature of the Pierre Shale and Fox Hills Formation has allowed for development of a high resolution biostratigraphic and chronostratigraphic framework for the Late Cretaceous WIS based on molluscan macrofossils (primarily ammonoid cephalopod and inoceramid bivalve mollusks) and radiometric dating of volcanic ash horizons (bentonites; Cobban et al., 2006).

Of the nine concretions from this study, five late Campanian concretions come from the *Baculites compressus* zone of the Pierre Shale in South Dakota. This biozone has been dated to ~73.8 Ma by Landman et al. (2018b). Abundant methane cold seeps occur in the WIS during this time interval (Gao et al., 2021; Landman et al., 2018a; Rowe et al., 2020), and samples were selected from both a known methane seep and non-seep locality for comparison. All *B. compressus* zone samples are from offshore localities 150-250 km east of the WIS shoreline based on the reconstructions of Cobban et al. (1994).

The remaining four Maastrichtian concretions come from the *Hoploscaphites birklundae, Hoploscaphites nicolletii* and *Hoploscaphites nebrascensis* zones of both the Pierre Shale and the Fox Hills Formation in South Dakota and Wyoming. These samples were selected to represent both nearshore (Fox Hills Formation) and offshore (Pierre Shale) deposition during these time intervals, which can be dated to ~69 – 67 Ma (Hicks et al., 1999; Slattery et al., 2015). The

shoreline of the WIS migrated basin-ward during the Maastrichtian as indicated by the time-transgressive facies of the Fox Hills Formation (Landman et al., 2013; Landman and Waage, 1993), while offshore deposition (the Pierre Shale) continued in the center of the basin (Kennedy et al., 1998). Detailed information on stratigraphy and locations for each sample can be found in Table 1.

In preparation for geochemical analysis, fossil shell, sparry calcite infilling cracks and voids, or matrix-derived carbonate were identified by eye or using a bifocal microscope (Figure 2 and Figure S1). Fossil shell and void-filling and crack-filling sparry calcite were removed from the concretion by manual scraping using a scalpel. They were then reacted with 10% hydrogen peroxide at room temperature for 2-15 minutes until vigorous bubbling stopped to remove potential organic matter. The sample was subsequently rinsed three times in distilled water and then exposed to 5% sodium hypochlorite solution for less than 4 hours for additional removal of recalcitrant organic matter. The sample was again rinsed three times in distilled water and dried at 60 °C.

Mineralogical data was obtained through powdered XRD performed using a Rigaku D/teX X-ray diffractometer at the University of New Mexico. Jade® whole pattern fitting software was used to distinguish calcite and aragonite.

Stable Isotope Analysis

The $\delta^{13}C$, $\delta^{17}O$, and $\delta^{18}O$ values are reported in per mil (‰) using standard δ-notation (McKinney et al., 1950):

$$\delta^{13}C \text{ or } \delta^{x}O = \left(\frac{R_{sample}}{R_{standard}} - 1\right) \times 1000, \quad (1)$$

where x is either mass 17 or 18 and R is $^{13}C/^{12}C$ or $^{x}O/^{16}O$. Oxygen isotope values are reported on the VSMOW scale while the $\delta^{13}C$ values are on the VPDB scale. The $\delta^{13}C$ and $\delta^{18}O$ analyses

were performed both in the Center for Stable Isotopes at the University of New Mexico (CSI-UNM) and in the Department of Geosciences stable isotope laboratory at Stony Brook University (SBU). The $\delta^{13}C$ and $\delta^{18}O$ values were obtained via conventional isotope ratio mass spectrometer (IRMS) analysis using phosphoric acid digestion (Spötl and Vennemann, 2003). Comparison of the $\delta^{13}C$ and $\delta^{18}O$ values can be found in the Supplementary File (Figure S10).

Triple oxygen isotope values were measured at CSI-UNM following the method described in Wostbrock et al. (2020b). In summary, five milligrams of powdered carbonate were loaded in nickel reaction vessels and reacted with bromine pentafluoride at 750 °C for 4 days. The oxygen (O_2) was quantitatively extracted and first cryogenically purified, then further purified in a 5A molecular sieve GC column before being analyzed in a Thermo Scientific MAT 253+ IRMS. The O_2 was analyzed relative to an in-house oxygen reference gas calibrated to VSMOW2-SLAP2 in dual inlet mode for 30 iterations with 28 sec integration times. Fluorination results in more variable, and generally lower, $\delta^{18}O$ values than measurements using a Gasbench-IRMS; however, any potential fractionation occurring during the reaction follows a slope of ~0.528 and does not impact the $\Delta'^{17}O$ values (Wostbrock et al., 2020a; Wostbrock et al., 2020b). Therefore, we use the $\Delta'^{17}O$ value obtained by fluorination and the $\delta^{18}O$ value obtained via the Gasbench-IRMS (Wostbrock et al., 2020a; Wostbrock et al., 2020b). To calculate the $\Delta'^{17}O$ values, we linearize the $\delta^{17}O$ and $\delta^{18}O$ values (Hulston and Thode, 1965; Miller, 2002), denoted using $\delta'^{17}O$ and $\delta'^{18}O$ and defined as:

$$\delta'^{x}O = 1000 ln\left(\frac{\delta^{x}O}{1000} + 1\right). \quad (2)$$

We use the $\delta'^{17}O$ and $\delta'^{18}O$ values to calculate the $\Delta'^{17}O$ value using the equation (Sharp and Wostbrock, 2021):

$$\Delta'^{17}O = (\delta'^{17}O - 0.528 \times \delta'^{18}O) \times 1000. \quad (3)$$

All $\Delta'^{17}O$ values are reported in ppm on the VSMOW2-SLAP2 scale (Wostbrock et al., 2018). Since replicates were limited due to samples size constraints, we assume a $\Delta'^{17}O$ error of ±10 ppm for all samples in this data, derived from the long-term 1σ standard deviation of the laboratory standards.

Carbonate clumped isotope analyses (Δ_{47}) were performed at SBU and carbonate clumped isotope temperatures ($T(\Delta_{47})$) are calculated using the equation (Petersen et al., 2019):

$$\Delta_{47} = \frac{0.0383 \times 10^6}{T^2} + 0.17, \quad (4)$$

where T is temperature in Kelvin. Δ_{47} values are reported in per mil units, and error is reported to the 95% confidence level. The Δ_{47} measurements were made using the method described in Gao et al. (2021). Briefly, 5-7 mg aliquots of powdered carbonate were reacted with phosphoric acid at 90 °C for 10 min. The CO_2 was constantly collected in a liquid nitrogen trap after passing through a -80 °C water trap. The CO_2 was then passed through a GC column for purification, concentrated on a cold finger, and analyzed in dual inlet mode on a Thermo Scientific MAT 253+ IRMS. Samples were analyzed against a reference CO_2 gas for 20 sec of sample integration for 10 iterations seven times (for a total of 70 iterations), corrected using thermally equilibrated CO_2 gases (Dennis et al., 2011), and compared with carbonate standards, some with internationally accepted Δ_{47} values (Bernasconi et al., 2021).

Fluid-Rock Mixing Model

We model trajectories of $\Delta'^{17}O$ and $\delta^{18}O$ during carbonate-water exchange due to fluid-rock interaction (diagenesis with a meteoric fluid) using the mass-balance model modified from

Taylor (1978) to include $\delta^{17}O$. The bulk composition of the system is the mass balance between the initial and final water and rock oxygen isotope compositions following the equation:

$$X_{water}\left(\delta^{x}O_{water,final}\right) + (1 - X_{water})\left(\delta^{x}O_{rock,final}\right) = \delta^{x}O_{bulk} =$$

$$X_{water}\left(\delta^{x}O_{water,intial}\right) + (1 - X_{water})\left(\delta^{x}O_{rock,intial}\right), \quad (5)$$

where X_{water} is the fraction of water and x is either mass 17 or 18. The $\delta^{x}O_{rock,final}$ requires an estimate of the $\alpha_{rock\text{-}water}$ value, where

$$\propto_{rock-water} = \frac{1000+\delta^{x}O_{final,rock}}{1000+\delta^{x}O_{final,water}}. \quad (6)$$

The $\alpha_{rock\text{-}water}$ value varies with temperature following the equation (Wostbrock et al., 2020a):

$$1000ln\alpha^{17}_{calcite-water} = \left(\frac{2.84\times10^{6}}{T^{2}} - 2.96\right)\left(\frac{-1.39}{T} + 0.5305\right), \quad (7)$$

for oxygen-17, and

$$1000ln\alpha^{18}_{carbonate-water} = \frac{2.84\times10^{6}}{T^{2}} - 2.96 \quad (8)$$

for oxygen-18. Note that we use "carbonate-water" in Eq. 8 since the same equation applies to both aragonite-water and calcite-water (Wostbrock et al., 2020a); however, this equation may not apply to other carbonate mineralogy such as dolomite. Combining Eq. 5 and 6 yields the calculation for $\delta^{x}O_{rock,final}$ (Wostbrock and Sharp, 2021):

$$\delta^{x}O_{rock,final} = \frac{1000X_{water}+\propto_{rock-water}\left(X_{water}\delta^{x}O_{rock,inital}-X_{water}\delta^{x}O_{water,inital}-\delta^{x}O_{rock,inital}-1000X_{water}\right)}{\propto_{rock-water}X_{water}-\propto-X_{water}}. \quad (9)$$

Two equations are calculated for $\delta^{17}O_{rock,final}$ and $\delta^{18}O_{rock,final}$ values and then are converted to prime notation for $\Delta'^{17}O$ calculations.

We can use this fluid-rock mixing model framework to back-calculate the initial temperature in which the shell mineralization occurred in altered samples. For this, we assume a time-integrated average temperature of alteration, a $\Delta'^{17}O$ and $\delta^{18}O$ value of the diagenetic fluid, and the $\Delta'^{17}O$ and $\delta^{18}O$ value of the seawater. The initial carbonate mineralogy of the shell

material was aragonite, thus the fractionation between aragonite and water was used to calculate the initial triple oxygen isotope composition of the mineral using Eq. 8 for the $\delta^{18}O$ value and the $\delta^{17}O$ using the aragonite-water fractionation equation from Wostbrock et al. (2020a):

$$1000ln\alpha^{17}_{aragonite-water} = \left(\frac{2.84\times10^{6}}{T^{2}} - 2.96\right)\left(\frac{-1.53}{T} + 0.5305\right). \quad (10)$$

For clarification, Eq. 7, which is for calcite-water fractionation, is used to represent alteration from aragonite mineralogy to calcite mineralogy during the fluid-rock interaction while Eq. 10 is used to represent initial aragonite mineralogy.

We used a Particle Swarm Optimization algorithm (PSO) available in the Python (3.x) pyswarm package to solve the fluid-rock mixing model (Eq. 7-10) and find the best values of alteration temperature, alteration fluid $\delta^{18}O$, and initial formation temperature to describe the measured $\Delta'^{17}O$ values. In general, a PSO uses multiple particles (referred to as a swarm) and iterates through a field of parameters (in this study: alteration temperature, alteration fluid $\delta^{18}O$, and initial formation temperature) applied to a set of equations (in this study, the fluid-rock mixing model) to minimize the residual between the modeled data and the observed (or measured) data. We used a swarm size of 100 particles and allowed the PSO to iterate up to 500 times to find the minimal residuals. The PSO usually found the optimized parameters within 10-60 iterations. Residuals were defined as the sum of the absolute difference between the measured $\Delta'^{17}O$ values of our dataset and the modeled $\Delta'^{17}O$ values from the fluid-rock mixing model calculated from the parameters of the PSO. The PSO iterates through the fluid-rock mixing model using different parameters until the difference of the residuals between iterations are below a threshold value (we used the default value of 10e-8) after which the PSO considers no more appreciable decrease in residuals will occur and outputs the optimized parameters. A PSO may provide slightly different optimized parameters after each run since the PSO stops iterating

294 over the parameter space when the difference between iterations falls below a certain threshold.
295 With enough runs, the PSO will have moved towards the optimized parameter from many
296 different angles within the parameter space, giving a range of optimized parameters that all
297 minimize the residuals of the set of equations equally. We recorded the optimized parameters
298 from 1000 PSO runs to capture the entire range of possible optimized values that minimize the
299 residuals of the fluid rock mixing model.

300 We set each parameter's upper and lower limits so that the PSO could only choose values
301 between those limits for each iteration. We set a wider range for the parameters than expected so
302 that the PSO would not find an optimized parameter at the end of the set parameter space. For
303 alteration temperatures, a temperature range of 0-75 °C was used. We chose this range to
304 accommodate the range of burial temperatures the concretion may have experienced during
305 alteration. If the alteration occurred close to the sediment-water interface, the temperature would
306 be similar to the bottom water temperature (minimum of ~0 °C) while later alteration after burial
307 would follow the geothermal gradient and increased temperature. We set a maximum burial
308 temperature of 75°C based on Denver Basin well temperatures and burial rates from Simon et al.
309 (2023), which is near our sampling locations and taken to be roughly representative. Alteration
310 fluid $\delta^{18}O$ values correspond with potential meteoric water $\delta^{18}O$ values (-20-0‰). We chose this
311 range based on the lowest $\delta^{18}O$ value (~-20‰) suggested by Fricke et al. (2010) if there was high
312 topography to the west of the WIS during the Late Cretaceous. We chose 0‰ as the highest $\delta^{18}O$
313 value for the alteration fluid to represent precipitation in warm, humid conditions with low
314 topography. Lastly, we set the initial shell precipitation temperature to a range of 0-45°C to
315 represent a larger range then expected temperatures based on the minimum temperature of
316 bottom water (0°C) and the maximum temperature results from this study (maximum

317 temperature reported is ~40°C). We calculated the meteoric water $\delta'^{17}O$ value using Eq. 8 from
318 Aron et al. (2021) to represent the global meteoric water line ($\delta'^{17}O = 0.5268 \times \delta'^{18}O + 0.015$)
319 and assumed a paleo-ocean $\delta^{18}O$ and $\Delta'^{17}O$ value of -1‰ and -0.002‰ (-2 ppm), respectively.
320 Setting a wider parameter space for each parameter results in a slower model and results in
321 model output that are unrealistic due to known analyses (such as maximum burial temperature,
322 see Figures S8 and S9 for more discussion). The ancient ocean $\delta^{18}O_{seawater}$ value was not used as
323 a parameter because changing that value from +2‰ to -3‰ does not change results as much as
324 the other three parameters (Figure S7 in Supplementary File). More information on the PSO
325 deployment and convergence can be found in the Supplementary File.

326 **RESULTS**

327 Four bivalve shells, seven ammonite shells, and four void/crack filling carbonate
328 (referred to as sparry calcite) samples were analyzed (Table 1). Based on XRD data on the shell
329 material, most samples have a majority of aragonite as the carbonate component (67-100%;
330 Table 2). The exception was sample UNM15525 (an unidentified bivalve) which was mostly
331 calcite (83%) and has a small component of silica (3%). The silica portion could not be separated
332 from the carbonate portion of the sample before fluorination for $\Delta'^{17}O$ analysis. Therefore, the
333 $\Delta'^{17}O$ value of sample UNM15525 has a minor silica contribution.

334 The $\delta^{13}C$ values of the skeletal aragonite range between -6.57 to +1.92‰ (VPDB; Figure
335 3; Tables 3 and 4). The skeletal aragonite from the locations known to contain methane seeps
336 generally have $\delta^{13}C$ values of <-5.4‰. The exceptions are UNM15502-1 and UNM15504-2
337 which are found in concretions near seeps and have $\delta^{13}C$ values of -3.33 and -3.78‰,
338 respectively. Non-seep related fossils have $\delta^{13}C$ values that ranged from -3.87 to +1.92‰. In all
339 cases where the comparison can be made, the $\delta^{13}C$ of the sparry calcite is considerably lower

than the fossil shells. They range from -18.34 to -13.60‰, regardless of whether the concretion came from a seep location or not. The low $\delta^{13}C$ value of the sparry calcite is best explained by oxidation of organic matter or formation near a methane seep where the $\delta^{13}C$ value could still be impacted. None of the $\delta^{13}C$ values are indicative of direct formation within methane seeps where anerobic oxidation of methane results in $\delta^{13}C$ values as low as -40‰ (Gao et al., 2021; Landman et al., 2018a; Rowe et al., 2020). Late Cretaceous ammonoids frequently have $\delta^{13}C$ values at least 4‰ lower than other carbonate secreting species found in the same location regardless of proximity to known methane seeps (Landman et al., 2018a; Landman and Klofak, 2012; Tobin and Ward, 2015). Several explanations have been proposed for the lower $\delta^{13}C$ values. They could indicate that the ammonoids were not residing full time within seep conditions, resulting in an intermediate $\delta^{13}C$ value representing both seep and non-seep conditions (Landman et al., 2018a; Landman and Klofak, 2012). Alternatively, ammonoids rapid growth rate may require higher metabolic rates and more CO_2 released during respiration than the smaller co-habitating organism (e.g., mollusks), resulting in lower $\delta^{13}C$ values of their shells (McConnaughey et al., 1997; Tobin and Ward, 2015).

The $\delta^{18}O$ values of the shells ranged from 26.48 to 30.86‰ (VSMOW; -4.30 to -0.05‰ vs. VPDB, where $\delta^{18}O_{VSMOW}=1.03092\times\delta^{18}O_{PDB}+30.92$ (Kim et al., 2015); Tables 3 and 4), similar to the reported range in Maastrichtian and Campanian ammonites from the Western Interior Seaway and Gulf Coastal Plain (Cochran et al., 2010; Knoll et al., 2016; Witts et al., 2020). The $\delta^{18}O$ values of the infill are generally 5-10‰ lower than the corresponding $\delta^{18}O$ values of the shell comparable to the sparry calcite veins and nodules from WIS methane seep concretions (Gao et al., 2021). The $\Delta'^{17}O$ value of samples ranged from -102 to -60 ppm (Table 4; Figure 4). Although there are no $\Delta'^{17}O$ values from the WIS to compare to the values in this

study, modern calcitic brachiopod $\Delta'^{17}O$ values range from -96 ppm at 0°C to -55 ppm at 40°C while aragonitic corals and sediment range from -114 ppm at 0°C and -67 ppm at 40°C (Wostbrock et al., 2020a). Except for sample AMNH161248, all infill components have higher $\Delta'^{17}O$ values than the corresponding shell material.

Measured Δ_{47} values range between 0.556 and 0.595‰ for the fossil shell samples and 0.556 to 0.608‰ for the sparry infill. These data correspond to temperatures ranging between 23 and 42 °C, with no obvious correlation with age or carbonate phase (Table 3; Figure 5). The Δ_{47} values of the infill carbonate always resulted in lower calculated water $\delta^{18}O$ relative to shell, showing that the infill has interacted to a larger extent with a low $\delta^{18}O$ diagenetic fluid. Calculated $\delta^{18}O$ values of the formation water (Eq. 8) using Δ_{47} values and assuming equilibrium isotope fractionation, range from -9.0 to +3.1‰ (Table 3).

We used the $\Delta'^{17}O$ and $\delta^{18}O$ values of the dataset in a particle swarm optimization algorithm (PSO) to determine formation temperatures and whether there are any temperature differences between the Campanian and Maastrichtian samples (Figures 7-8). The calculated seawater temperature was 22-25°C when considering the entire dataset in the PSO. Within each time period, we separate the dataset into higher and lower temperature bins based on the shell $\Delta'^{17}O$ values to capture the entire range of possible seawater temperatures. We consider $\Delta'^{17}O$ values below -70 ppm as "low temperature", which corresponds to seawater 30°C and below, for a $\delta^{18}O_{seawater}$ value of -1‰. This is to separate samples whose $\Delta'^{17}O$ values alone suggest temperatures that are at or near the maximum temperature for ectotherms (Pörtner, 2002). For the Campanian sample set, seawater temperatures range between 25 and 38°C while for the Maastrichtian sample set, seawater temperatures range between 9 and 28°C.

DISCUSSION

Here we investigate the utility of the combined measurements of $\Delta'^{17}O$, $\delta^{18}O$, and Δ_{47} along with quantitative modeling to document/calculate diagenetic alteration and increase the accuracy of geochemical reconstructions of paleoenvironmental conditions. Some carbonate concretions in this study have void-filling and crack-filling calcite, taken to represent a later stage carbonate that formed from fluids (most likely meteoric water per the results of the fluid-rock mixing model) interacting with the concretion after burial. This is further inferred using the XRD data that shows that some original aragonite had been replaced with calcite in the shell carbonate of some originally aragonitic fossils (Table 2). We interpret the aragonite identified by XRD to most likely represent the shell formed during ammonite growth while the presence of any calcite in the fossil to represent transformation from aragonite to calcite during diagenesis. To explore the extent diagenesis affected the $\Delta'^{17}O$, $\delta^{18}O$, and Δ_{47} of the fossil ammonite and bivalve shells, we use the $\Delta'^{17}O$ and $\delta^{18}O$ values to distinguish between pristine vs. altered shell samples (Figure 4). For the altered shells, we see through the alteration by using a fluid-rock mixing model to estimate the primary precipitation temperature. Lastly, we discuss the implications of interpreting the fossil $\Delta'^{17}O$, $\delta^{18}O$, and Δ_{47} values without correcting for any diagenesis.

Using $\Delta'^{17}O$ and $\delta^{18}O$ Values to Distinguish Between Pristine vs. Altered Samples

The $\delta^{18}O_{seawater}$ and $\Delta'^{17}O_{seawater}$ Values that Represent WIS Oceanic Conditions

The seawater $\Delta'^{17}O$ and $\delta^{18}O$ range that we consider reasonable ocean conditions during the Late Cretaceous is shown in the yellow bar in Figure 4. During a greenhouse climate with no polar ice caps present, the average $\delta^{18}O_{seawater}$ value is assumed to be -1‰ (Shackleton and Kennett, 1975) and the $\Delta'^{17}O_{seawater}$ value is assumed to -2 ppm (McGunnigle et al., 2022), compared to an average of 0‰ and -5 ppm, for $\delta^{18}O_{seawater}$ and $\Delta'^{17}O_{seawater}$ respectively, in the

409 modern ocean where some ice caps are present (Craig and Gordon, 1965; Luz and Barkan,
410 2010). However, local variations are possible due to local evaporation and/or influx of meteoric
411 water (Kelson et al., 2022; LeGrande and Schmidt, 2006; Petersen et al., 2016; Schmidt et al.,
412 1999). Therefore, we adapted the modern $\delta^{18}O$ range of surface seawater (-2 to +2‰; Schmidt et
413 a., 1999) to greenhouse conditions (-3 to +1 ‰) to give a range that could represent WIS
414 seawater (yellow line, Figure 4). This is similar to the range of WIS $\delta^{18}O_{seawater}$ values calculated
415 from Δ_{47} values in other studies (Dennis et al., 2013; Gao et al., 2021; Jones et al., 2022; Petersen
416 et al., 2016). The corresponding $\Delta'^{17}O$ values of the endmember seawater $\delta^{18}O$ values do not
417 change appreciably from the average seawater $\Delta'^{17}O$ value (-2 ppm). A 20% addition of meteoric
418 water with a $\delta^{18}O$ value of -12‰ is required to change the WIS $\delta^{18}O_{seawater}$ value from -1‰ to -
419 3‰. Using a canonical meteoric water $\Delta'^{17}O$ value of 0.03‰ would result in a $\Delta'^{17}O_{seawater}$
420 increase of only 4 ppm. On average, the $\Delta'^{17}O$ value of residual evaporated water decreases by
421 ~2 ppm per 1‰ increase in $\delta^{18}O$ values for a change in $\delta^{18}O$ of less than 5‰ (Huth et al., 2022).
422 For evaporation to cause an increase in the WIS $\delta^{18}O_{seawater}$ value to 1‰, the $\Delta'^{17}O_{seawater}$ value
423 would decrease by 4 ppm to -8 ppm. The range of WIS $\Delta'^{17}O_{seawater}$ and $\delta^{18}O_{seawater}$ values is
424 therefore represented by the yellow bar in Figure 4.

425 ***The Aragonite-Water Triple Oxygen Isotope Equilibrium Fractionation Field***

426 Triple oxygen isotope values of geologic samples provide information on the oxygen
427 isotope composition and temperature of the fluid in which the sample formed because there is
428 only one equilibrium carbonate $\Delta'^{17}O$ and $\delta^{18}O$ value for a given temperature and seawater $\Delta'^{17}O$
429 and $\delta^{18}O$ value. To determine whether the $\Delta'^{17}O$ and $\delta^{18}O$ values of the fossil carbonate preserve
430 primary marine conditions or have experienced post-deposition alteration, we calculated a field
431 of equilibrium carbonate triple oxygen isotope values that represent precipitation in modern

seawater, adapted to a Cretaceous greenhouse climate (Figure 4). We discuss how we calculate the seawater-carbonate equilibrium field below. Fossil carbonate $\Delta'^{17}O$ and $\delta^{18}O$ values that plot within this field are considered unaltered, or 'pristine', and record initial temperature of precipitation and the $\Delta'^{17}O$ and $\delta^{18}O$ value of the seawater in which it formed. Fossil carbonate that does not have $\Delta'^{17}O$ and $\delta^{18}O$ values that plot within this field are altered and no longer preserve the initial environmental conditions in which it formed. Their isotopic composition may, however, be used to back-calculate original conditions.

The carbonate-water triple oxygen isotope fractionation equation has been determined empirically (Wostbrock et al., 2020a) and theoretically (Guo and Zhou, 2019; Hayles et al., 2018; Schauble and Young, 2021), with the empirical estimate being within error of all the theoretical estimates. Theoretical fractionation calculations for temperatures between 0 and 100 °C show about a 0.5‰ difference for the $\delta^{18}O$ fractionation and little to no difference in the $\Delta'^{17}O$ fractionation between calcite-water and aragonite-water (Schauble and Young, 2021), although the empirical results from four modern aragonite samples indicate a slightly lower $\Delta'^{17}O$ fractionation relative to calcite (e.g., 18 ppm lower at 0 °C; Wostbrock et al., 2020b). Since XRD results indicate the biogenic carbonate is majority aragonite, we used the aragonite-water triple oxygen isotope calibration curve to describe primary precipitation environments for this dataset, which yields the equation:

$$\Delta'^{17}_{Arg} - \Delta'^{17}_{wt} = \left(\frac{2.84(\pm 0.02)\times 10^6}{T^2} - 2.96(\pm 0.19)\right)\left(\frac{-1.53(\pm 0.2)}{T} + 0.5305 - \lambda\right), \quad (11)$$

where T is temperature in Kelvin and λ is the reference slope taken as 0.528 in this work (Sharp et al., 2018). Supplementary materials show the dataset recalculated using the calcite-water fractionation curve from Wostbrock et al. (2020a) and results in calculated temperatures about 10°C cooler than when using aragonite-water (Eq. 11).

455 The triple oxygen aragonite-water equilibrium fractionation line corresponding to an
456 ocean with a $\delta^{18}O$ value of -1‰ and $\Delta'^{17}O$ value of -2 ppm is shown in Figure 4 (black line). The
457 aragonite-water equilibrium fractionation field corresponding to an ocean with $\delta^{18}O$ values of -
458 3‰ and +1‰ is denoted by the grey field in Figure 4. If the $\Delta'^{17}O$ and $\delta^{18}O$ values of the fossil
459 carbonate samples from this study are only a function of their habitat/formation temperature in
460 seawater, then their $\Delta'^{17}O$ and $\delta^{18}O$ values should lie within the field in Figure 4. If a fossil
461 carbonate sample lies outside this field, it has been altered by interaction with meteoric or pore
462 waters (Wostbrock and Sharp, 2021). By using this range of $\delta^{18}O_{seawater}$ values, we interpret all
463 fossil carbonate samples from this study that have $\Delta'^{17}O$ and $\delta^{18}O$ values falling between a
464 $\delta^{18}O_{seawater}$ value of -3 and +1 ‰ as pristine and unaltered.

465 ***Campanian Concretions (*Baculites Compressus *Biozone)***

466 Based on our triple oxygen isotope results, the fossils within non-seep concretions
467 correspond to about 1‰ lower $\delta^{18}O_{seawater}$ values than fossils within the three concretions from
468 known methane seep localities (Table 4 and Figure 4A). All concretions were retrieved from the
469 Pierre Shale, commonly interpreted as an offshore depositional setting. Although the sample size
470 is small, this could indicate that the higher carbon content and early cementation in sediments
471 proximal to WIS cold methane seeps hinders the potential for diagenetic resetting, a phenomenon
472 which warrants further investigation (see Landman et al. (2018a) and Gao et al. (2021)).

473 ***Offshore, non-seep concretions.*** Two shells from the ammonite *Baculites compressus*
474 were analyzed from two different concretions (UNM15473 and UNM15505). The ammonite in
475 concretion UNM15505 (UNM15505-1) has a triple oxygen isotope composition that corresponds
476 to a $\delta^{18}O_{seawater}$ value of -3‰ and formed at a temperature of 22°C (Figure 4A). The ammonite in
477 concretion UNM15473 has a $\Delta'^{17}O$ value that are within error of the $\Delta'^{17}O$ value of UNM15505-

1 and a $\delta^{18}O$ value that correspond to a $\delta^{18}O_{seawater}$ value of -2‰ (Figure 4A). Concretion sample UNM15505 also contained secondary sparry infill. Void-filling sparry calcite was sampled from within a *Baculites compressus* (UNM15505-2; Figure 2A) fossil while a crack-filling sparry calcite was sampled from within a crosscutting crack (UNM15505-3; Figure 2B). The $\Delta'^{17}O$ and $\delta^{18}O$ values of the infill samples all indicate interaction with a light meteoric fluid (Figure 4A and 4C). Clumped isotope temperatures for these samples range between 27-35°C, with the sparry infill recording the highest of these temperatures (Figure 5).

Offshore, methane seep locality concretions. The three near-seep concretions contained a variety of mollusk species. UNM15503 contained a single planispiral ammonite fossil: an incomplete specimen of *Placenticeras meeki*. UNM15504 contained both lucinid and inoceramid bivalves. UNM15502 contained a scaphitid ammonite (*Hoploscaphites* sp.), inoceramid bivalves, and void-filling sparry calcite of a small indeterminate fossil. The oxygen isotope compositions of fossil shell samples consistently show equilibrium precipitation with $\delta^{18}O_{seawater}$ values between -1 and -3‰ (+/- 2‰; Figure 4A). The $\delta^{18}O$ and $\Delta'^{17}O$ values of the void-filling sparry calcite (UNM15502-2) are evidence of interaction with a light meteoric water (Figure 4A).

Two fossils (UNM15503-1 – *Placenticeras meeki* and UNM15504-1 – lucinid bivalve) have $\delta^{18}O$ and $\Delta'^{17}O$ values that correspond to a temperature >30°C; while the remaining fossils (UNM15502 - *Hoploscaphites* sp. and two inoceramid bivalves) have $\delta^{18}O$ and $\Delta'^{17}O$ values that correspond to a temperature between 20-25°C (Figure 4A). The difference in temperatures could be related to habitat. *Placenticeras meeki* may have lived higher in the water column (>30°C) than *Hoploscaphites* sp. (20-30°C), which may have been adapted to mid to lower water column and nektobenthic habitats (Landman et al., 2018a; Tsujita and Westermann, 1998). Potentially, the temperature difference between the two ammonite species could indicate thermal

501 stratification of the Late Cretaceous WIS with warmer surface water and cooler temperatures at
502 depth. More specimens would be required before making definitive statements about thermal
503 stratification.

504 There are multiple explanations for the temperature difference between the two different
505 bivalve species. In terms of habitats, inoceramids are typically found lying parallel to bedding,
506 suggesting they did not burrow and lived at the sediment-water interface (MacLeod and Hoppe,
507 1992). Lucinid bivalves were infaunal burrowers that live in the sediment with high organic
508 carbon content (Taylor et al., 2014) where temperature may be slightly elevated compared to the
509 bottom water-sediment interface. Modern lucinid bivalves are known to host sulfur-oxidizing
510 bacterial symbionts and burrow to high sulfur concentrations in sediments (Bryant et al., 2023).
511 Neither diagenesis nor vital effects can explain the difference in the bivalve samples. Evaluating
512 so-called "vital effects" is important when considering whether biogenic carbonate precipitated
513 in isotopic equilibrium. Although empirical studies of how vital effects may impact triple oxygen
514 isotope values have not yet been explored, we find it unlikely that a vital effect would result in
515 an equilibrium triple oxygen isotope value, as seen in the bivalve fossils in this study (Figure 4).
516 Theoretical work has shown that vital effects caused through the (de)hydroxylation of
517 bicarbonate imposes a kinetic, non-equilibrium fractionation effect and would result in the shell
518 carbonate having either lower $\Delta'^{17}O$ and $\delta^{18}O$ values (in the case of hydroxylation) or higher
519 $\Delta'^{17}O$ and $\delta^{18}O$ values (in the case of dehydroxylation) from the equilibrium carbonate value
520 (Figure 4E; Guo and Zhou, 2019). Similarly, diagenesis would not result in a carbonate that has a
521 $\Delta'^{17}O$ and $\delta^{18}O$ value that plots within our carbonate-water equilibrium field (as shown by the
522 fluid-rock mixing model). Since the fossil bivalve triple oxygen isotope values fall within the
523 equilibrium carbonate-water field (Figure 4), and until more systematic studies have been

524 performed, we assume vital effects or diagenesis did not impact these samples and the observed
525 temperature difference is environmental.
526 For Campanian samples that have measured values for both paired $\delta^{18}O$-$\Delta'^{17}O$ and Δ_{47}
527 values, the temperatures calculated from Δ_{47} ($T(\Delta_{47})$) are equal to or higher than those using
528 $\delta^{18}O$-$\Delta'^{17}O$ thermometry ($T(\Delta'^{17}O)$); Tables 3 and 4; Figures 4-6). The *Placenticeras meeki*
529 (UNM15503-1) and *Baculites compressus* (UNM15505-1) fossils have reconstructed
530 temperatures that are within error between the two isotope systems, ($T(\Delta'^{17}O)$= 33°C (±10);
531 $T(\Delta_{47})$=42°C (±7) and $T(\Delta'^{17}O)$ = 22°C (±10); $T(\Delta_{47})$=27°C (±6), respectively) (Tables 3 and 4).
532 This suggests the ~10°C difference in formation temperatures is real and the Campanian WIS
533 had thermal heterogeneity.
534 A $\Delta'^{17}O$-Δ_{47} equilibrium fractionation line was calculated using equations 4 and 11 (black
535 line, Figure 6). Samples that formed in equilibrium with seawater should have Δ_{47} and $\Delta'^{17}O$
536 values that correspond to the calculated $\Delta'^{17}O$-Δ_{47} equilibrium line for a given temperature. Note,
537 however, that using the $\Delta'^{17}O$-Δ_{47} equilibrium line for temperature estimates results in large
538 errors. Therefore, we only use the $\Delta'^{17}O$-Δ_{47} equilibrium line to look at how the two values relate
539 to one another and explore processes that may have impacted the observed values and do not
540 derive any temperature information from the $\Delta'^{17}O$-Δ_{47} equilibrium line. Campanian fossil shells
541 UNM15503-1 and UNM15505-1 have $\Delta'^{17}O$ and Δ_{47} values that plot within measurement error
542 (interpreted by the error bars) on the $\Delta'^{17}O$-Δ_{47} equilibrium fractionation line. Void-filling and
543 crack-filling sparry calcite samples (UNM15502-2 and UNM15505-2) also have similar $\Delta'^{17}O$-
544 Δ_{47} temperatures (Figure 6), which we interpret to reflect fluid-rock interaction that affected
545 $\Delta'^{17}O$, $\delta^{18}O$, and Δ_{47} values in such a way that maintained isotopic equilibrium at the diagenetic

conditions. The T(Δ_{47}) values are within the range of fossil reconstructed T(Δ_{47}) (42 and 35°C for UNM15502-2 and UNM15505-2, respectively; Table 3). However, these samples clearly do not reflect marine conditions as shown by their $\Delta'^{17}O$-$\delta^{18}O$ values (Figure 4). Therefore we interpret this temperature to reflect a minimum temperature of alteration, indicating that these concretions may have formed rapidly after burial, preserving near marine conditions as suggested by previous studies (Landman and Klofak, 2012; Maples, 1986; Zatoń and Marynowski, 2006).

Maastrichtian Concretions

One *Hoploscaphites* sp. fossil (UNM15526-1) has a $\Delta'^{17}O$ and $\delta^{18}O$ value that corresponds to a formation temperature of 32°C (+/- 10°C; Figure 4B) in waters of ~1.5‰ (+/- 2‰). Another *Hoploscaphites* sp. fossil (AMNH161248-4) has the same temperature of formation but suggests formation in 2.6‰ (+/-2) water, outside of our previously defined field of unaltered values. The ammonite T(Δ_{47}) in concretion AMNH161248 is 35°C, indistinguishable from 32°C using $\Delta'^{17}O$-$\delta^{18}O$ thermometry. The AMNH161248 concretion also has void-filling sparry calcite that does not plot within the ice-free $\delta^{18}O$ range of seawater (Figure 4B). The $\Delta'^{17}O$ value of the sparry infill is considerably lower than the fossil, suggesting a late-stage diagenetic fluid that formed inside the shell at lower temperature than the fossil growth conditions. The Δ_{47} value also suggests a lower temperature of formation for the void-filling sparry calcite (23°C) vs. the fossil shell (35°C).

The remaining fossil samples from the nearshore basal Fox Hills Formation of the *Hoploscaphites birklundae* zone in Red Bird, Wyoming (UNM 15525) and the offshore Elk Butte Member of the Pierre Shale of the *Hoploscaphites nicolletii* zone in South Dakota (AMNH 46620) did not plot within the range of an ice-free seawater indicating some alteration has

occurred. A highly silicified concretion (UNM15525-1) had the highest $\Delta'^{17}O$ and lowest $\delta^{18}O$ values, indicating that it was clearly altered. The $T(\Delta_{47})$ reconstruction supports this conclusion. The sample yielded a low calculated water $\delta^{18}O$ value (-7.9‰) and warm (albeit within the range of reported temperatures from this study) $T(\Delta_{47})$ of 38°C (Table 3).

"Seeing Through" Diagenesis from Altered Fossil Carbonate

We used the multiple carbonate phases (fossil and crack-filling and void-filling sparry calcite) from this study to constrain the diagenetic history of the carbonate concretions using a fluid-rock mixing model in a PSO algorithm (see Methods and Results sections for more information). Histograms of the PSO output show the range of alteration temperatures, meteoric water values, and formation temperatures that best describe the dataset from this study (Figure 7 and 8). Most optimized alteration temperatures range between 45 and 70 °C. However, the optimized formation temperatures occupy a narrow range based on the dataset used. When considering the entire dataset, most of the PSO results suggest a formation temperature of 25 °C (ranging between 22 and 25°C; Figure 7). Breaking the dataset up into time periods and samples that have higher or lower $\Delta'^{17}O$ values, the formation temperatures change (Figure 8). The Maastrichtian samples have formation temperatures that range from 9 to 27°C. The Campanian samples have formation temperatures that range between 25 and 38°C. This suggests a potential cooling of the ocean during the Maastrichtian, similar (albeit larger total change) to global sea surface temperature changes interpreted from TEX_{86} and benthic foraminifera $\delta^{18}O$ global records (Huber et al., 2018; O'Brien et al., 2017).

We assume that the diagenetic fluids that altered the carbonate are meteoric in origin. Therefore, the PSO output for the alteration fluid $\delta^{18}O$ value is ultimately set by paleo-precipitation $\delta^{18}O$ values. We find that paleo-precipitation $\delta^{18}O$ values between -12 and -9 ‰

592 best describes all the data (Figure 7). The optimized $\delta^{18}O$ value is lower when the alteration
593 temperature is also lower and is higher as the alteration temperature increases closer to 75°C (see
594 supplementary file). When analyzing the dataset by the high and low temperature groups within
595 each time period, the high temperature Campanian group had alteration fluid $\delta^{18}O$ values lower
596 than the average dataset (-14 to -11 ‰) and the low temperature Maastrichtian group had
597 alteration fluid $\delta^{18}O$ values higher than the average dataset (-10 to -7 ‰) (Figure 8). Although
598 different from each other, these results still overlap with the average $\delta^{18}O$ value of the alteration
599 fluid from the entire dataset. Paleo-precipitation $\delta^{18}O$ value of -12 to -9‰ is slightly higher than
600 the -20 to -14‰ proposed in Fricke et al. (2010) to represent high elevation recharge during
601 summer monsoons. However, the low $\delta^{18}O$ value of -12 to -9 ‰ must represent some extent of
602 paleo-elevation as proposed in Fricke et al. (2010) and Poulsen et al. (2007) since precipitation
603 sourced through evaporation of nearby seawater without significant elevation change would have
604 considerably higher $\delta^{18}O$ values. Therefore, to achieve paleo-precipitation $\delta^{18}O$ values of -12 to -
605 9 ‰ requires the infiltration of fluids sourced from higher elevations into the shallow sediments
606 at the time of early carbonate diagenesis.

607 **Implications of Interpreting Habitat Environments using Fossil Shell $\Delta'^{17}O$, $\delta^{18}O$, and Δ_{47}**
608 **Values without Correcting for any Diagenesis**

609 Overall, if the Δ_{47} values are taken as primary, there is no difference in temperature or
610 $\delta^{18}O_{seawater}$ values between the two periods and the positive WIS $\delta^{18}O_{seawater}$ value was a result of
611 evaporation, which increases the $\delta^{18}O$ value of a water body. The Δ_{47} values of the fossil
612 carbonate reflect $\delta^{18}O_{seawater}$ values of >0‰ and temperatures ≥35°C except for AMNH46620-1
613 ($T(\Delta_{47})$ = 31°C; offshore, Maastrichtian sample) and UNM15505-1 ($T(\Delta_{47})$ = 27°C; non-seep,

614 Campanian sample; Figure 4). The highest T(Δ_{47}) is 42°C from UNM15503-1 (near-seep,
615 Campanian sample; Figure 4).

616 The $\Delta'^{17}O$ and $\delta^{18}O$ values of the fossil carbonate reflect a similar temperature story as
617 the Δ_{47} values but the opposite story regarding the WIS $\delta^{18}O_{seawater}$ values. The WIS $\delta^{18}O_{seawater}$
618 value must be between -7‰ and +3‰ for all fossil carbonate in this study to reflect initial
619 precipitation environments (Figures 4C and 4D). Similar to the Δ_{47} values, there is no difference
620 in the range of $\delta^{18}O_{seawater}$ values between either the Campanian or Maastrichtian samples. The
621 two samples that reflect low $\delta^{18}O_{seawater}$ values (UNM15473 and AMNH46620) also correspond
622 to the lowest temperatures (≤10°C; Figure 4C and 4D). The Maastrichtian samples that reflect
623 higher $\delta^{18}O_{seawater}$ values also reflect higher temperatures (~40°C; Figure 4D). Although the
624 $\delta^{18}O_{seawater}$ range is not too different from other reported values (Petersen et al., 2016), a
625 $\delta^{18}O_{seawater}$ value of -7‰ is unlikely. The WIS would require an input of 50% freshwater with a
626 $\delta^{18}O$ value of -12‰ to change the $\delta^{18}O_{seawater}$ value from -1‰ to -7‰ (Figure 4C and 4D). Such
627 a flux of freshwater would require ammonites and other cephalopods living in these regions to be
628 insensitive to a 50% drop in salinity, challenging the existing paleobiological paradigm for these
629 taxa. Additionally, the only <-7‰ $\delta^{18}O_{seawater}$ value derived from the Δ_{47} values were from a void
630 filling calcite sample (UNM15505-2; Figure 5), taken to represent an alteration fluid and not
631 seawater. Based on the fossil triple oxygen isotope values, we cannot interpret all fossil data
632 from this study to reflect original habitat or environmental conditions and conclude that
633 diagenesis impacted the isotopic composition of some of the fossils enough to represent
634 sedimentary burial environments.

635 **Resolving the Δ_{47} and $\Delta'^{17}O$ Values of This Study**

For our study, the paired $\Delta'^{17}O$-Δ_{47} data further validates the samples that were deemed pristine based on their $\delta^{18}O$-$\Delta'^{17}O$ values plotting within the equilibrium field from Figure 4 (UNM15505-1, UNM15503-1) and the ~10°C difference in formation temperature between the two samples is robust. Two samples (UNM15526-1 and AMNH161248-4) have $\Delta'^{17}O$-Δ_{47} values that are within error of the $\Delta'^{17}O$-Δ_{47} equilibrium line but do not plot within the triple oxygen isotope equilibrium field. We interpret this as further support of evaporation affecting the WIS seawater $\delta^{18}O$ value, resulting in a higher $\delta^{18}O_{seawater}$ value during the Maastrichtian. Reconstructed $\delta^{18}O_{seawater}$ values for UNM15526-1 and AMNH161248-4 are 2.6‰ (±1.5) and 3.1‰ (±1.2) using Δ_{47} values and 1.7‰ (±2) and 2.8‰ (±2) using $\delta^{18}O$-$\Delta'^{17}O$ values, respectively. A Campanian fossil (UNM15502-1) has $\delta^{18}O$-$\Delta'^{17}O$ values that fall within the triple oxygen equilibrium field but does not appear be in $\Delta'^{17}O$-Δ_{47} equilibrium (Figure 6). We are confident that, based on the triple oxygen isotope values, this sample is pristine and reflects similar formation temperatures and $\delta^{18}O_{seawater}$ values as other pristine samples from the Campanian dataset (UNM15502-4, UNM15504-2, and UNM15505-1; Figures 4B and 4D). Therefore, this sample may have Δ_{47} values that have been altered by a process that does not impact the $\delta^{18}O$ or $\Delta'^{17}O$ values, mainly a process that involved little fluid interaction such that $\delta^{18}O$ and $\Delta'^{17}O$ were unaffected. The $T(\Delta_{47})$ and $\delta^{18}O_{seawater}$ values are reasonable (37°C and 1.3‰, respectively); however the $\delta^{18}O$-$\Delta'^{17}O$ reconstructed temperature and $\delta^{18}O_{seawater}$ (23°C and 1.3‰, respectively) reveals that the sample actually reflects the low temperature group of the Campanian fossils. This demonstrates the usefulness of paired $\Delta'^{17}O$-Δ_{47} values to distinguish small differences within a dataset. Fossils AMNH46620-1 and UNM15473-1 and infill sample

AMNH161248-1 all have $\Delta'^{17}O$-Δ_{47} values that are not in equilibrium, similar to Figure 4 using $\delta^{18}O$-$\Delta'^{17}O$ values.

It is possible, but not presently well known whether, vital effects could impact the $\Delta'^{17}O$, $\delta^{18}O$, and Δ_{47} values differently. Metabolic vital effects have been shown to impact $\delta^{13}C$ values of fast-growing ammonites (McConnaughey et al., 1997; Tobin and Ward, 2015). Clumped isotope measurements in high shell growth areas of modern cephalopods, *Nautilus* sp., have yielded lower Δ_{47} values (i.e., higher $T(\Delta_{47})$) than predicted from ambient seawater temperature, though the available studies are hampered by legacy clumped isotope data correction issues (e.g., Dennis et al., 2013) or poorly known thermal histories for the studied specimens (i.e., Nautilus are known to make large diurnal migrations from cooler deep waters to the warmer surface, and back; Davies et al., 2021; Dunstan et al., 2011). Cephalopod aragonite may be an example of negligible $\delta^{18}O$ vital effect offsets and potentially important Δ_{47} vital effect offsets (Davies et al., 2021; Dennis et al., 2013). Additional research is needed to fully evaluate whether Δ_{47} values that appear too warm in fossil taxa are related to these vital effects, burial alteration, or some combination of both.

As described earlier when discussing vital effects in bivalves, it is unknown how vital effects impact triple oxygen isotope values. If the vital effect causes non-equilibrium precipitation due to the hydroxylation or dehydroxylation of bicarbonate (through changes in CO_2), then the carbonate triple oxygen isotope composition is expected to deviate from expected equilibrium with either lower $\Delta'^{17}O$ and $\delta^{18}O$ (for hydroxylation) or higher $\Delta'^{17}O$ and $\delta^{18}O$ values (for dehydroxylation; Figure 4E). We cannot attribute vital effects impacting the triple oxygen isotope values of biogenic carbonate that plot within the triple oxygen equilibrium field (Figure 4) because we do not, as of yet, have a vital effect mechanism that would cause equilibrium

680 precipitation. Therefore, we interpret those oxygen isotope values as primary and reflecting
681 initial precipitation conditions. Minor hydroxylation disequilibrium vital effects overlap minor
682 diagenesis effects (Figure 4E). Therefore, we cannot distinguish between vital effects or meteoric
683 diagenesis for samples UNM15502-1, UNM15473-1, and AMNH46620-1. However, combined
684 with the void-filling and crack-filling sparry calcite samples that we know formed through
685 meteoric water infiltration, 'seeing through' diagenesis still adequately describes those samples.
686 A clear observation from all our data is that fossil shell clumped isotope temperatures are
687 mostly higher (albeit usually within error) than those from triple oxygen isotopes (Figures 4 and
688 5). However, many of the fossil shell $\delta^{18}O$ and $\Delta'^{17}O$ values that plot within the seawater
689 equilibrium field (Figure 4) have $\Delta'^{17}O$-Δ_{47} temperatures that plot within measurement error
690 (error bars) of the $\Delta'^{17}O$-Δ_{47} equilibrium line (Figure 6). Samples that have $\Delta'^{17}O$ and Δ_{47} values
691 that plot on the $\Delta'^{17}O$-Δ_{47} equilibrium line but do not have $\Delta'^{17}O$-$\delta^{18}O$ values that plot within the
692 carbonate-water equilibrium field (namely, the void and crack filling sparry calcite samples
693 UNM15502-2 and UNM15505-2), reflect re-equilibration at high fluid-rock ratios impacting the
694 $\Delta'^{17}O$, $\delta^{18}O$, and Δ_{47} values and are not a reflection of primary temperatures.
695 The analytical challenge of triple oxygen and clumped isotope analysis means that they
696 are infrequently measured on the same samples. Future work focusing on the co-analysis of the
697 two systems in a variety of carbonate-forming settings may be illustrative of their co-dependence
698 (or not). The $\Delta'^{17}O$-Δ_{47} equilibrium line combines two independent variables as an additional
699 check on diagenesis. This could be particularly useful in samples where the reconstructed
700 clumped isotope temperature is either slightly high or slightly lower than expected and it is
701 unclear whether some other process may have impacted the isotope values (as is the case for
702 samples UNM15502-1, UNM15473-1, and AMNH46620-1, Figure 6).

Implications for Oceanographic Reconstructions of the Late Cretaceous WIS

Temperature (20-40°C) and $\delta^{18}O_{seawater}$ (-3 – 0‰) values from the triple oxygen isotopes and most of the clumped isotope measurements in this study overlap with clumped isotope temperatures for the Campanian derived by previous carbonate analyses from the Western Interior Seaway (Figure 9; Dennis et al., 2013; Gao et al., 2021; Petersen et al., 2016). For the Maastrichtian WIS, our temperatures are similar, albeit cooler, to those of Petersen et al. (2016) and Dennis et al. (2013) (10-25°C, this study, vs. ~20°C, previous studies). However, the WIS $\delta^{18}O_{seawater}$ values reported in this study are slightly higher than those reported in Petersen et al. (2016) and Dennis et al. (2013). We do not think that this represents a non-homogenous WIS during the Maastrichtian as suggested in Petersen et al. (2016) because ~50% of the seawater would need to be freshwater to change the WIS $\delta^{18}O_{seawater}$ value to -6‰ and would drastically change the salinity of the WIS and habitability for marine organisms (Figures 4 and 9). Alternatively, the potentially shallower Maastrichtian WIS would result in higher $\delta^{18}O_{seawater}$ values due to evaporation, as suggested by the triple oxygen isotope values of the Maastrichtian fossils. An expansion of the Maastrichtian datasets with the inclusion of careful $\Delta'^{17}O$ and Δ_{47} analyses are necessary to determine the difference in connectedness of the WIS to the open ocean during the early and late Maastrichtian.

CONCLUSIONS

Through this study, we show that primary paleoenvironmental information can be deconvolved from even minor diagenetic effects by combining $\Delta'^{17}O$, $\delta^{18}O$, and Δ_{47} measurements of fossil carbonate. Additionally, we can ‘see through’ diagenesis by measuring additional carbonate phases, such as void-filling or crack-filling calcite and estimate initial precipitation environments in altered fossil carbonates. This combined measurement approach

allows for better characterization of paleoenvironmental conditions in the Late Cretaceous North American Western Interior Seaway (WIS); our results are not only useful for paleoceanographic reconstructions, but also investigations of environment-life interactions in an important marine system leading into a major mass extinction.

Based on the data from this study, we make the following conclusions regarding the Late Cretaceous WIS:

1. Average temperatures of the WIS were between 20 and 40°C. Temperatures from fossil shells are 10-40°C from triple isotope constraints and 26 to 42°C from clumped isotopes. Results of the Particle Swarm Optimization (PSO) suggest the temperature of the Maastrichtian WIS was 10-15 °C cooler than during the Campanian.
2. Maastrichtian seawater may have been restricted and affected by more evaporation (resulting in a higher $\delta^{18}O$ value) than Campanian seawater (which has similar $\delta^{18}O$ values expected of the open ocean in a primarily ice-free Cretaceous world).
3. The WIS during the Campanian may have been thermally stratified with ~10°C warmer surface water and cooler bottom water. This is supported by both Δ_{47} and $\delta^{18}O$-$\Delta'^{17}O$ values and PSO results.
4. Diagenesis occurred via the infiltration of meteoric water into the carbonate concretions. All the void-filling and crack-filling calcite (in the form of sparry infill) in the concretions interacted with a light meteoric water (~ -10‰), suggesting moderate topographic relief on the western coast of the WIS or that groundwater represented a mixture of high and low altitude precipitation (Fricke et al., 2010; Poulsen et al., 2007). We confirm that he sparry calcite from these concretions are not a good proxy for

determining primary Cretaceous ocean temperatures, but do provide important information on burial conditions and diagenetic history of the region.

5. Both the PSO and paired $\Delta'^{17}O$-Δ_{47} values support that the carbonate concretions from this dataset formed and were altered rapidly after shallow burial in temperatures of ~40°C.

ACKNOWLEDGEMENTS

We thank Neil Landman (AMNH) and Kirk Cochran (Stony Brook University) for useful discussions on WIS paleoceanography and Bushra Husseini (AMNH) for access to collections and facilitating the loan of fossil material used in our study. We thank Viorel Atudorei (UNM) for thoughtful discussions about data interpretation. We thank Mark Brandon (Yale) for discussion on the utility of the Particle Swarm Optimization Algorithm. J.A.G.W would like to acknowledge funding from NSF grants DGE-1418062 and NSF EAR PF-1952615. Z.D.S. and J.A.G.W acknowledges funding from NSF grant #1551226. C.E.M would like to acknowledge funding from NSF grant #1601878.

REFERENCES

Aron, P.G., Levin, N.E., Beverly, E.J., Huth, T.E., Passey, B.H., Pelletier, E.M., Poulsen, C.J., Winkelstern, I.Z., Yarian, D.A., 2021. Triple oxygen isotopes in the water cycle. Chem. Geol. 565, 120026.

Arthur, M.A., Dean, W.E., Schlanger, S.O., 1985. Variations in the Global Carbon Cycle During the Cretaceous Related to Climate, Volcanism, and Changes in Atmospheric CO2, in: Sundquist, E.T., Broecker, W.S. (Eds.), The Carbon Cycle and Atmospheric CO2: Natural Variations Archean to Present. American Geophysical Union Geophysical Monograph, pp. 504-529.

Banner, J.L., Hanson, G.N., 1990. Calculation of simultaneous isotopic and trace element variations during water-rock interaction with applications to carbonate diagenesis. Geochim. Cosmochim. Acta 54, 3123-3137.

Barrera, E., Savin, S.M., 1999. Evolution of late Campanian-Maastrichtian marine climates and oceans. Geological Society of America Special Paper 332, 245-282.

Bernasconi, S.M., Daëron, M., Bergmann, K.D., Bonifacie, M., Meckler, A.N., Affek, H.P., Anderson, N., Bajnai, D., Barkan, E., Beverly, E., Blamart, D., Burgener, L., Calmels, D., Chaduteau, C., Clog, M., Davidheiser-Kroll, B., Davies, A., Dux, F., Eiler, J., Elliott, B., Fetrow, A.C., Fiebig, J., Goldberg, S., Hermoso, M., Huntington, K.W., Hyland, E., Ingalls, M., Jaggi, M., John, C.M., Jost, A.B., Katz, S., Kelson, J., Kluge, T., Kocken, I.J., Laskar, A., Leutert, T.J., Liang, D., Lucarelli, J., Mackey, T.J., Mangenot, X., Meinicke, N., Modestou, S.E., Müller, I.A., Murray, S., Neary, A., Packard, N., Passey, B.H., Pelletier, E., Petersen, S., Piasecki, A., Schauer, A., Snell, K.E., Swart, P.K., Tripati, A., Upadhyay, D., Vennemann, T., Winkelstern, I., Yarian, D., Yoshida, N.,

786 Zhang, N., Ziegler, M., 2021. InterCarb: A Community Effort to Improve Interlaboratory
787 Standardization of the Carbonate Clumped Isotope Thermometer Using Carbonate
788 Standards. Geochemistry, Geophysics, Geosystems 22, e2020GC009588.
789 Brusatte, S.L., Butler, R.J., Barrett, P.M., Carrano, M.T., Evans, D.C., Lloyd, G.T., Mannion,
790 P.D., Norell, M.A., Peppe, D.J., Upchurch, P., Williamson, T.E., 2015. The extinction of
791 the dinosaurs. Biological Reviews 90, 628-642.
792 Bryant, R.N., Richardson, J.A., Kalia, T.C., Gros, O., Lopez-Garriga, J., Blättler, C.L., 2023.
793 Inorganic sulfate–based signatures of chemosymbiosis in modern infaunal lucinids.
794 Geology 51, 1022-1026.
795 Clarke, L.J., Jenkyns, H.C., 1999. New oxygen isotope evidence for long-term Cretaceous
796 climatic change in the Southern Hemisphere. Geology 27, 699-702.
797 Cobban, W.A., Mereweather, E.A., Fouch, T.D., Obradovich, J.D., 1994. Some Cretaceous
798 shorelines in the Western Interior of the United States, in: Caputo, M.V., Peterson, J.A.,
799 Franczyk, K.J. (Eds.), Mesozoic Systems of the Rocky Moutain region. SEPM Rocky
800 Mountain Section, Denver, USA.
801 Cobban, W.A., Walaszczyk, I., Obradovich, J.D., McKinney, K.C., 2006. A USGS Zonal Table
802 for the Upper Cretaceous Middle Cenomanian-Maastrichtian of the Western Inerior of
803 the United States Based on Ammonites, Inoceramids, and Radiometric Ages. U.S
804 Geological Survey Open-File Report 2006-1250, 1-45.
805 Cochran, J.K., Kallenberg, K., Landman, N.H., Harries, P.J., Weinreb, D., Turekian, K.K., Beck,
806 A.J., Cobban, W.A., 2010. Effect of diagenesis on the Sr, O, and C isotope composition
807 of late Cretaceous mollusks from he Western Interior Seaway of North America.
808 American Journal of Science 310, 69-88.

809 Cochran, J.K., Landman, N.H., Turekian, K.K., Michard, A., Schrag, D.P., 2003.
810 Paleoceanography of the Late Cretaceous (Maastrichtian) Western Interior Seaway of
811 North America: evidence from Sr and O isotopes. Palaeogeography, Palaeoclimatology,
812 Palaeoecology 191, 45-64.
813 Condamine, F.L., Guinot, G., Benton, M.J., Currie, P.J., 2021. Dinosaur biodiversity declined
814 well before the asteroid impact, influenced by ecological and environmental pressures.
815 Nat Commun 12, 3833.
816 Coulson, A.B., Kohn, M.J., Barrick, R.E., 2011. Isotopic evaluation of ocean circulation in the
817 Late Cretaceous North American seaway. Nature Geoscience 4, 852-855.
818 Craig, H., Gordon, L.I., 1965. Deuterium and oxygen 18 variations in the ocean and the marine
819 atmosphere, in: Tongiorgi, E. (Ed.), Stable isotopes in oceanographic studies and
820 paleotemperatures, Spoleto, pp. 9-130.
821 Davies, A.J., Davis, S., John, C.M., 2021. Evidence of taxonomic non-equilibrium effects in the
822 clumped isotope composition of modern cephalopod carbonate. Chem. Geol. 578,
823 120317.
824 Dennis, K.J., Affek, H.P., Passey, B.H., Schrag, D.P., Eiler, J.M., 2011. Defining an absolute
825 reference frame for ‘clumped’ isotope studies of CO2. Geochim. Cosmochim. Acta 75,
826 7117-7131.
827 Dennis, K.J., Cochran, J.K., Landman, N.H., Schrag, D.P., 2013. The climate of the Late
828 Cretaceous: New insights from the application of the carbonate clumped isotope
829 thermometer to Western Interior Seaway macrofossil. Earth and Planetary Science
830 Letters 362, 51-65.

831 Dennis, K.J., Schrag, D.P., 2010. Clumped isotope thermometry of carbonatites as an indicator
832 of diagenetic alteration. Geochim. Cosmochim. Acta 74, 4110-4122.
833 Dunstan, A.J., Ward, P.D., Marshall, N.J., 2011. Vertical Distribution and Migration Patterns of
834 Nautilus pompilius. PLOS ONE 6, e16311.
835 Eiler, J.M., 2011. Paleoclimate reconstruction using carbonate clumped isotope thermometry.
836 Quaternary Science Reviews 30, 3575-3588.
837 Fricke, H.C., Foreman, B.Z., Sewall, J.O., 2010. Integrated climate model-oxygen isotope
838 evidence for a North American monsoon during the Late Cretaceous. Earth and Planetary
839 Science Letters 289, 11-21.
840 Gao, Y., Henkes, G.A., Cochran, J.K., Landman, N.H., 2021. Temperatures of Late Cretaceous
841 (Campanian) methane-derived authigenic carbonates from the Western Interior Seaway,
842 South Dakota, USA, using clumped isotopes. GSA Bulletin.
843 Geraghty, M.D., Westermann, G.E.G., 1994. Origin of jurassic ammonite concretions
844 assemblages at Alfeld, Germany: a biogenic alternative. Paläontologische Zeitschrift 68,
845 473-490.
846 Gill, J.R., Cobban, W.A., 1966. The Red Bird section of the Upper Cretaceous Pierre Shale of
847 Wyoming. U.S Geological Survey Professional Paper 393-A, 1-73.
848 Guo, W., Zhou, C., 2019. Triple oxygen isotope fractionation in the DIC-H_2O-CO_2 system: A
849 numerical framework and its implications. Geochim. Cosmochim. Acta 246, 541-564.
850 Hay, W., Eicher, D., Diner, R., 1993. Physical oceanography and water masses of the Cretaceous
851 Western Interior Seaway, in: Caldwell, W.G.E., Kauffman, E.G. (Eds.), Evolution of the
852 Western Interior Basin. Geological Association of Canada Special Paper, pp. 297-318.

Hay, W.W., 2008. Evolving ideas about the Cretaceous climate and ocean circulation. Cretaceous Res. 29, 725-753.

Hayles, J., Gao, C., Cao, X., Liu, Y., Bao, H., 2018. Theoretical calibration of the triple oxygen isotope thermometer. Geochim. Cosmochim. Acta 235, 237-245.

He, S., Kyser, T.K., Caldwell, W.G.E., 2005. Paleoenvironment of the Western Interior Seaway inferred from δ18O and δ13C values of molluscs from the Cretaceous Bearpaw marine cyclothem. Palaeogeography, Palaeoclimatology, Palaeoecology 217, 67-85.

Hemingway, J.D., Henkes, G.A., 2021. A disordered kinetic model for clumped isotope bond reordering in carbonates. Earth and Planetary Science Letters 566, 116962.

Henkes, G.A., Passey, B.H., Grossman, E.L., Shenton, B.J., Pérez-Huerta, A., Yancey, T.E., 2014. Temperature limits for preservation of primary calcite clumped isotope paleotemperatures. Geochim. Cosmochim. Acta 139, 362-382.

Hicks, J.F., Obradovich, J.D., Tauxe, L., 1999. Magnetostratigraphy, isotopic age calibration and intercontinental correlation of the Red Bird section of the Pierre Shale, Niobrara County, Wyoming, USA. Cretaceous Res. 20, 1-27.

Huber, B.T., Hodell, D.A., Hamilton, C.P., 1995. Middle–Late Cretaceous climate of the southern high latitudes: Stable isotopic evidence for minimal equator-to-pole thermal gradients. GSA Bulletin 107, 1164-1191.

Huber, B.T., MacLeod, K.G., Watkins, D.K., Coffin, M.F., 2018. The rise and fall of the Cretaceous Hot Greenhouse climate. Global Planet. Change 167, 1-23.

Huber, B.T., Norris, R.D., MacLeod, K.G., 2002. Deep-sea paleotemperature record of extreme warmth during the Cretaceous. Geology 30, 123-126.

875 Hulston, J.R., Thode, H.G., 1965. Variations in the S^{33}, S^{34}, and S^{36} contents of meteorites and
876 their relation to chemical and nuclear effects. Journal of Geophysical Research 70, 3475-
877 3484.
878 Huntington, K.W., Petersen, S.V., 2023. Frontiers of Carbonate Clumped Isotope Thermometry.
879 Annu. Rev. Earth Planet. Sci. 51, 611-641.
880 Huth, T.E., Passey, B.H., Cole, J.E., Lachniet, M.S., McGee, D., Denniston, R.F., Truebe, S.,
881 Levin, N.E., 2022. A framework for triple oxygen isotopes in speleothem
882 paleoclimatology. Geochim. Cosmochim. Acta 319, 191-219.
883 Jones, M.M., Petersen, S.V., Curley, A.N., 2022. A tropically hot mid-Cretaceous North
884 American Western Interior Seaway. Geology.
885 Kauffman, E., 1984. Paleobiogeography and evolutionary response dynamic in the Cretaceous
886 Western Interior Seaway of North America, in: Westermann, G.E.G. (Ed.), Jurassic–
887 Cretaceous Biochronology and Paleogeography of North America: Geological
888 Association of Canada Special Paper, pp. 273-306.
889 Kauffman, E., Caldwell, W., 1993. The Western Interior Basin in space and time. Geological
890 Association of Canada Special Paper 39.
891 Kelson, J.R., Petersen, S.V., Niemi, N.A., Passey, B.H., Curley, A.N., 2022. Looking upstream
892 with clumped and triple oxygen isotopes of estuarine oyster shells in the early Eocene of
893 California, USA. Geology 50, 755-759.
894 Kennedy, W.J., Landman, N.H., Christensen, W.K., Cobban, W.A., Hancock, J.M., 1998.
895 Marine connections in North America during the late Maastrichtian: palaeogeographic
896 and palaeobiogeographic significance ofJeletzkytes nebrascensisZone cephalopod fauna

from the Elk Butte Member of the Pierre Shale, SE South Dakota and NE Nebraska. Cretaceous Res. 19, 745-775.

Kim, S.-T., Coplen, T.B., Horita, J., 2015. Normalization of stable isotope data for carbonate minerals: Implementation of IUPAC guidelines. Geochim. Cosmochim. Acta 158, 276-289.

Knoll, K., Landman, N.H., Cochran, J.K., Macleod, K.G., Sessa, J.A., 2016. Microstructural preservation and the effects of diagenesis on the carbon and oxygen isotope composition of Late Cretaceous aragonitic mollusks from the Gulf Coastal Plain and the Western Interior Seaway. American Journal of Science 316, 591-613.

Landman, N., Cochran, J., Slovacek, M., Larson, N., Garb, M., Brezina, J., Witts, J., 2018a. Isotope sclerochronology of ammonites (Baculites Compressus) from methane seep and non-seep sites in the Late Cretaceous Western Interior Seaway, USA: Implications for ammonite habitat and mode of life. American Journal of Science 318, 603-639.

Landman, N., Remin, Z., Garb, M., Jr, J., 2013. Cephalopods from the Badlands National Park area, South Dakota: Reassessment of the position of the Cretaceous/Paleogene boundary. Cretaceous Res. 42, 1–27.

Landman, N.H., Goolaerts, S., Jagt, J.W.M., Jagt-Yazykova, E.A., Machalski, M., 2015. Ammonites on the Brink of Extinction: Diversity, Abundance, and Ecology of the Order Ammonoidea at the Cretaceous/Paleogene (K/Pg) Boundary, in: Klug, C., Korn, D., De Baets, K., Kruta, I., Mapes, R.H. (Eds.), Ammonoid Paleobiology: From macroevolution to paleogeography. Springer Netherlands, Dordrecht, pp. 497-553.

Landman, N.H., Jicha, B.R., Cochran, J.K., Garb, M.P., Brophy, S.K., Larson, N.L., Brezina, J., 2018b. 40Ar/39Ar date of a bentonite associated with a methane seep deposit in the upper

Campanian Baculites compressus Zone, Pierre Shale, South Dakota. Cretaceous Res. 90, 90-96.

Landman, N.H., Klofak, S.M., 2012. Anatomy of a concretion: Life, death, and burial in the Western Interior Seaway. Palaios 27, 672-693.

Landman, N.H., Waage, K.M., 1993. Scaphitid ammonites of the Upper Cretaceous (Maastrichtian) Fox Hills Formation in South Dakota and Wyoming. Bulletin of the American Museum of Natural History.

LeGrande, A.N., Schmidt, G.A., 2006. Global gridded data set of the oxygen isotopic composition in seawater. Geophysical Research Letters 33.

Looser, N., Petschnig, P., Hemingway, J.D., Fernandez, A., Morales Grafulha, L., Perez-Huerta, A., Vickers, M.L., Price, G.D., Schmidt, M.W., Bernasconi, S.M., 2023. Thermally-induced clumped isotope resetting in belemnite and optical calcites: Towards material-specific kinetics. Geochim. Cosmochim. Acta 350, 1-15.

Luz, B., Barkan, E., 2010. Variations of $^{17}O/^{16}O$ and $^{18}O/^{16}O$ in meteoric waters. Geochim. Cosmochim. Acta 74, 6276-6286.

MacLeod, K.G., Hoppe, K.A., 1992. Evidence that inoceramid bivalves were benthic and harbored chemosynthetic symbionts. Geology 20, 117-120.

Maples, C.G., 1986. Enhanced Paleoecological and Paleoenvironmental Interpretations Result from Analysis of Early Diagenetic Concretions in Pennsylvanian Shales. Palaios 1, 512-516.

McConnaughey, T.A., Burdett, J., Whelan, J.F., Paull, C.K., 1997. Carbon isotopes in biological carbonates: Respiration and photosynthesis. Geochim. Cosmochim. Acta 61, 611-622.

McGunnigle, J.P., Cano, E.J., Sharp, Z.D., Muehlenbachs, K., Cole, D., Hardman, M.F., Stachel, T., Pearson, D.G., 2022. Triple oxygen isotope evidence for a hot Archean ocean. Geology 50, 991-995.

McKinney, C.R., McCrea, J.M., Epstein, S., Allen, H.A., Urey, H.C., 1950. Improvements in mass spectrometers for the measurement of small differences in isotope abundance ratios. Review of Scientific Instruments 21, 724-730.

Miall, A.D., Catuneanu, O., Vakarelov, B.K., Post, R., 2008. Chapter 9 The Western Interior Basin, in: Miall, A.D. (Ed.), Sedimentary Basins of the World. Elsevier, pp. 329-362.

Miller, M.F., 2002. Isotopic fractionation and the quantification of ^{17}O anomalies in the oxygen three-isotope system: an appraisal and geochemical significance. Geochim. Cosmochim. Acta 66, 1881-1889.

O'Brien, C.L., Robinson, S.A., Pancost, R.D., Sinninghe Damsté, J.S., Schouten, S., Lunt, D.J., Alsenz, H., Bornemann, A., Bottini, C., Brassell, S.C., Farnsworth, A., Forster, A., Huber, B.T., Inglis, G.N., Jenkyns, H.C., Linnert, C., Littler, K., Markwick, P., McAnena, A., Mutterlose, J., Naafs, B.D.A., Püttmann, W., Sluijs, A., van Helmond, N.A.G.M., Vellekoop, J., Wagner, T., Wrobel, N.E., 2017. Cretaceous sea-surface temperature evolution: Constraints from TEX86 and planktonic foraminiferal oxygen isotopes. Earth-Science Reviews 172, 224-247.

Passey, B.H., Henkes, G.A., 2012. Carbonate clumped isotope bond reordering and geospeedometry. Earth and Planetary Science Letters 351-352, 223-236.

Petersen, S.V., Defliese, W.F., Saenger, C., Daëron, M., Huntington, K.W., John, C.M., Kelson, J.R., Bernasconi, S.M., Colman, A.S., Kluge, T., Olack, G.A., Schauer, A.J., Bajnai, D., Bonifacie, M., Breitenbach, S.F.M., Fiebig, J., Fernandez, A.B., Henkes, G.A., Hodell,

D., Katz, A., Kele, S., Lohmann, K.C., Passey, B.H., Peral, M.Y., Petrizzo, D.A., Rosenheim, B.E., Tripati, A., Venturelli, R., Young, E.D., Winkelstern, I.Z., 2019. Effects of Improved 17O Correction on Interlaboratory Agreement in Clumped Isotope Calibrations, Estimates of Mineral-Specific Offsets, and Temperature Dependence of Acid Digestion Fractionation. Geochemistry, Geophysics, Geosystems 20, 3495-3519.

Petersen, S.V., Tabor, C.R., Lohmann, K.C., Poulsen, C.J., Meyer, K.W., Carpenter, S.J., Erickson, J.M., Matsunaga, K.K.S., Smith, S.Y., Sheldon, N.D., 2016. Temperature and salinity of the Late Cretaceous Western Interior Seaway. Geology 44, 903-906.

Pörtner, H.O., 2002. Climate variations and the physiological basis of temperature dependent biogeography: systemic to molecular hierarchy of thermal tolerance in animals. Comparative Biochemistry and Physiology Part A: Molecular & Integrative Physiology 132, 739-761.

Poulsen, C.J., Pollard, D., White, T.S., 2007. General circulation model simulation of the δ18O content of continental precipitation in the middle Cretaceous: A model-proxy comparison. Geology 35, 199-202.

Raiswell, R., Fisher, Q.J., 2000. Mudrock-hosted carbonate concretions: a review of growth mechanisms and their influence on chemical and isotopic composition. Journal of the Geological Society 157, 239-251.

Raiswell, R., Fisher, Q.J., 2004. Rates of carbonate cementation associated with sulphate reduction in DSDP/ODP sediments: implications for the formation of concretions. Chem. Geol. 211, 71-85.

Reeside, J.B., Cobban, W.A., 1960. Studies of the Mowry shale (Cretaceous) and contemporary formations in the United States and Canada, Professional Paper, - ed.

Roberts, L.N.R., Kirschbaum, M.A., 1995. Paleogeography and the Late Cretaceous of the Western Interior of middle North America; coal distribution and sediment accumulation, Professional Paper, - ed.

Rowe, A., Landman, N., Cochran, J., Witts, J., Garb, M., 2020. Late Cretaceous methane seeps as habitats for newly hatched ammonites. Palaios 35, 151-163.

Royer, D.L., Berner, R.A., Beerling, D.J., 2001. Phanerozoic atmospheric CO2 change: evaluating geochemical and paleobiological approaches. Earth-Science Reviews 54, 349-392.

Ryb, U., Eiler, J.M., 2018. Oxygen isotope composition of the Phanerozoic ocean and a possible solution to the dolomite problem. Proceedings of the National Academy of Sciences 115, 6602-6607.

Sachs, J.P., Schwab, V.F., 2011. Hydrogen isotopes in dinosterol from the Chesapeake Bay estuary. Geochim. Cosmochim. Acta 75, 444-459.

Sakamoto, M., Benton, M.J., Venditti, C., 2016. Dinosaurs in decline tens of millions of years before their final extinction. Proceedings of the National Academy of Sciences 113, 5036-5040.

Schauble, E.A., Young, E.D., 2021. Mass Dependence of Equilibrium Oxygen Isotope Fractionation in Carbonate, Nitrate, Oxide, Perchlorate, Phosphate, Silicate, and Sulfate Minerals. Reviews in Mineralogy and Geochemistry 86, 137-178.

Schmidt, G., Bigg, G., Rohling, E., 1999. Global seawater oxygen-18 database. http://data.giss.nasa.gov/o18data.

1009 Shackleton, N.J., Kennett, J.P., 1975. Paleotemperature history of the cenozoic and the initiation
1010 of Antarctic glaciation: Oxygen and carbon isotope analyses in DSDP sites 277, 279, and
1011 281. DSDP Reports and Publicaitons XXIX, 743-755.
1012 Sharp, Z.D., Wostbrock, J.A.G., 2021. Standardization for the Triple Oxygen Isotope System:
1013 Waters, Silicates, Carbonates, Air, and Sulfates. Reviews in Mineralogy and
1014 Geochemistry 86, 179-196.
1015 Sharp, Z.D., Wostbrock, J.A.G., Pack, A., 2018. Mass-dependent triple oxygen isotope variations
1016 in terrestrial materials. Geochemical Perspectives Letters 7, 27-31.
1017 Shenton, B.J., Grossman, E.L., Passey, B.H., Henkes, G.A., Becker, T.P., Laya, J.C., Perez-
1018 Huerta, A., Becker, S.P., Lawson, M., 2015. Clumped isotope thermometry in deeply
1019 buried sedimentary carbonates: The effects of bond reordering and recrystallization. GSA
1020 Bulletin 127, 1036-1051.
1021 Simon, R.E., Budd, D.A., Snell, K.E., 2023. The history of calcite diagenesis and origin of
1022 exceptionally negative oxygen isotope values in chalks of the Niobrara Formation,
1023 Denver Basin, USA. The Depositional Record 9, 607-634.
1024 Slattery, J.S., Cobban, W.A., McKinney, K.C., Harries, P.J., Sandness, A.L., 2015. Early
1025 Cretaceous to Paleocene paleogeography of the Western Interior Seaway: the interaction
1026 of eustasy and tectonism, in: Bingle-Davis, M. (Ed.), Field guide, Cretaceous
1027 Conference: Evolution and Revolution. Wyoming Geological Association, Casper, WY,
1028 pp. 22-60.
1029 Slattery, J.S., Harries, P.J., Sandness, A.L., 2018. Do marine faunas track lithofacies? Faunal
1030 dynamics in the Upper Cretaceous Pierre Shale, Western Interior, USA.
1031 Palaeogeography, Palaeoclimatology, Palaeoecology 496, 205-224.

1032 Spötl, C., Vennemann, T.W., 2003. Continuous-flow isotope ratio mass spectrometric analysis of
1033 carbonate minerals. Rapid Communications in Mass Spectrometry 17, 1004-1006.
1034 Stinnesbeck, W., Ifrlm, C., Salazar, C., 2012. The Last Cretaceous Ammonites in Latin America.
1035 Acta Palaeontol. Pol. 57, 717-728.
1036 Stolper, D.A., Eiler, J.M., Higgins, J.A., 2018. Modeling the effects of diagenesis on carbonate
1037 clumped-isotope values in deep- and shallow-water settings. Geochim. Cosmochim. Acta
1038 227, 264-291.
1039 Taylor, H.P., 1978. Oxygen and hydrogen isotope studies of plutonic granitic rocks. Earth and
1040 Planetary Science Letters 38, 177-210.
1041 Taylor, J.D., Glover, E.A., Williams, S.T., 2014. Diversification of chemosymbiotic bivalves:
1042 origins and relationships of deeper water Lucinidae. Biol. J. Linn. Soc. 111, 401-420.
1043 Tierney, J.E., Poulsen, C.J., Montañez, I.P., Bhattacharya, T., Feng, R., Ford, H.L., Hönisch, B.,
1044 Inglis, G.N., Petersen, S.V., Sagoo, N., Tabor, C.R., Thirumalai, K., Zhu, J., Burls, N.J.,
1045 Foster, G.L., Goddéris, Y., Huber, B.T., Ivany, L.C., Kirtland Turner, S., Lunt, D.J.,
1046 McElwain, J.C., Mills, B.J.W., Otto-Bliesner, B.L., Ridgwell, A., Zhang, Y.G., 2020.
1047 Past climates inform our future. Science 370, eaay3701.
1048 Tobin, T.S., Ward, P.D., 2015. Carbon isotope (δ13C) differences between Late Cretaceous
1049 ammonites and benthic mollusks from Antarctica. Palaeogeography, Palaeoclimatology,
1050 Palaeoecology 428, 50-57.
1051 Tobin, T.S., Wilson, G.P., Eiler, J.M., Hartman, J.H., 2014. Environmental change across a
1052 terrestrial Cretaceous-Paleogene boundary section in eastern Montana, USA, constrained
1053 by carbonate clumped isotope paleothermometry. Geology 42, 351-354.

Tourtelot, H.A., Rye, R.O., 1969. Distribution of Oxygen and Carbon Isotopes in Fossils of Late Cretaceous Age, Western Interior Region of North America. GSA Bulletin 80, 1903-1922.

Tsujita, C.J., 1995. Origin of Concretion-Hosted Shell Clusters in the Late Cretaceous Bearpaw Formation, Southern Alberta, Canada. Palaios 10, 408-423.

Tsujita, C.J., Westermann, G.E.G., 1998. Ammonoid habitats and habits in the Western Interior Seaway: a case study from the Upper Cretaceous Bearpaw Formation of southern Alberta, Canada. Palaeogeography, Palaeoclimatology, Palaeoecology 144, 135-160.

Waage, K.M., 1964. Origin of repeated fossiliferous concretion layers in the Fox Hills Formation. Kansas Geological Survey Bulletin 169, 541-563.

Waage, K.M., 1968. The Type Fox Hills Formation, Cretaceous (Maestrichtian), South Dakota, Pt. 1, stratigraphy and paleoenvironments. Peabody Museum of Natural History Bulletin 27, 1-175.

Wang, S.C., Dodson, P., 2006. Estimating the diversity of dinosaurs. Proceedings of the National Academy of Sciences 103, 13601-13605.

Witts, J.D., Landman, N.H., Hopkins, M.J., Myers, C.E., 2020. Evolutionary stasis, ecophenotypy and environmental controls on ammonite morphology in the Late Cretaceous (Maastrichtian) Western Interior Seaway, USA. Palaeontology 63, 791-806.

Wostbrock, J.A.G., Brand, U., Coplen, T.B., Swart, P.K., Carlson, S.J., Brearley, A.J., Sharp, Z.D., 2020a. Calibration of carbonate-water triple oxygen isotope fractionation: Seeing through diagenesis in ancient carbonates. Geochim. Cosmochim. Acta 288, 369-388.

1075 Wostbrock, J.A.G., Cano, E.J., Sharp, Z.D., 2020b. An internally consistent triple oxygen isotope
1076 calibration of standards for silicates, carbonates and air relative to VSMOW2 and
1077 SLAP2. Chem. Geol. 533, 119432.
1078 Wostbrock, J.A.G., Sharp, Z.D., 2021. Triple Oxygen Isotopes in Silica–Water and Carbonate–
1079 Water Systems. Reviews in Mineralogy and Geochemistry 86, 367-400.
1080 Wostbrock, J.A.G., Sharp, Z.D., Sanchez-Yanez, C., Reich, M., van den Heuvel, D.B., Benning,
1081 L.G., 2018. Calibration and application of silica-water triple oxygen isotope thermometry
1082 to geothermal systems in Iceland and Chile. Geochim. Cosmochim. Acta 234, 84-97.
1083 Wright, E.K., 1987. Stratification and paleocirculation of the Late Cretaceous Western Interior
1084 Seaway of North America. GSA Bulletin 99, 480-490.
1085 Zatoń, M., Marynowski, L., 2006. Ammonite fauna from uppermost Bajocian (Middle Jurassic)
1086 calcitic concretions from the Polish Jura—biogeographical and taphonomical
1087 implications. Geobios 39, 426-442.
1088
1089

FIGURE CAPTIONS

Figure 1: Sample locality maps. Solid black lines represent reconstructed shorelines from Cobban et al. (1994) for the Campanian *Baculites compressus* and Maastrichtian *Baculites clinolobatus* Zones. White areas represent marine conditions. Grey shaded areas represent land. A) Campanian sample locations (yellow stars) from the offshore Pierre Shale formation in South Dakota. B) Maastrichtian sample locations (yellow stars) from the nearshore Fox Hills formation and the offshore Pierre Shale formation.

Figure 2: Photographs of three concretion hand samples from this study (door lock key for scale). A) and B) Concretion UNM15505 that contained an ammonite fossil (*Baculites compressus*) and 2 different types of sparry calcite infill. There are 2 types of infill sampled. Void filling calcite, which we define as calcite that precipitated inside fossil shells and crack filling calcite which precipitated generally in cross cutting cracks across the concretion. Note the cracks in these samples do not go to the rim of the concretion. In this concretion, the void filling calcite was only present near the fossil. A blocky, dark yellow/brown mineral (white arrow and labelled "not carbonate"), suspected to be a sulfur containing mineral such as barite, was also present in this void. C) Concretion AMNH46620 which represents a concretion with no crack or void filling calcite. D) Concretion UNM15504 which represents a fossiliferous concretion with different bivalve species. The arrow is pointing to a *Nymphalucina occidentalis* bivalve fossil (Sample UNM15504-1).

Figure 3: Carbon and oxygen isotope data for the WIS samples. Fossil shells (circles – ammonoids, diamonds – bivalves) have higher $\delta^{13}C$ and $\delta^{18}O$ values than the sparry infill (squares). The exception is UNM15525 which is highly silicified (red diamond). One sparry

1112 infill sample has a higher $\delta^{18}O$ value (AMNH161248, with a $\delta^{18}O$ value of ~31‰) but similar
1113 $\delta^{13}C$ of the other infill samples.
1114 Figure 4: Triple oxygen isotope compositions of late Campanian carbonate concretions for seep
1115 and non-seep localities within the *Baculites compressus* biozone (A, C) and early Maastrichtian
1116 carbonate concretions for nearshore and offshore localities (B, D). Panels A and B uses our
1117 defined WIS $\delta^{18}O$ values of -3 to +1‰ while Panels C and D reflect the WIS $\delta^{18}O$ values
1118 required if interpreting all fossil carbonate from this study as unaltered. The aragonite-water
1119 equilibrium fractionation field is represented by the gray field with the average global ocean
1120 $\delta^{18}O$ value of -1‰ represented by the black line. A, B) For a sample to be considered unaltered,
1121 the triple oxygen isotope composition of the fossil carbonate (circle and diamonds) must plot
1122 within the grey field defining the triple oxygen isotope equilibrium fractionation field for
1123 aragonite-water in equilibrium with an ocean with a $\delta^{18}O$ value of -3‰ to +1‰ (yellow bar). The
1124 late-stage void-filling and crack-filling calcite samples (squares) do not plot within the
1125 equilibrium field, suggesting alteration affected the triple oxygen isotope values. A highly
1126 silicified bivalve sample (UNM15525, red diamond) does not plot near the fractionation field,
1127 probably due to contamination. C, D) If all fossil carbonate from this study preserved primary
1128 $\Delta'^{17}O$ and $\delta^{18}O$ values, the calculated WIS seawater $\delta^{18}O$ value would range from -7‰ (left gray
1129 equilibrium fractionation line) to +3‰ (right gray equilibrium fractionation line). Seawater with
1130 a $\delta^{18}O$ value of -7‰ requires the addition of 50% freshwater with a $\delta^{18}O$ value of -12‰ (gray
1131 line with white dots). Using a simple Rayleigh fractionation model to represent evaporation, 20%
1132 of the seawater would need to evaporate to produce a $\delta^{18}O$ seawater value of 3‰. E) Schematic
1133 showing how the triple oxygen isotope composition of carbonate can be different from an
1134 expected equilibrium value (yellow circle). Evaporation results in a water with lower $\Delta'^{17}O$ and

higher $\delta^{18}O$ values; therefore, a carbonate precipitating in evaporated water would have lower $\Delta'^{17}O$ and higher $\delta^{18}O$ values lower than expected for carbonate precipitating in equilibrium with a more normal seawater oxygen isotope composition (purple arrow). Diagenesis by infiltration of a meteoric fluid will cause the carbonate triple oxygen isotope value to change following the blue arrow. The fluid-rock ratio controls where along the blue arrow the altered triple oxygen isotope value would plot. Note this is a general schematic and magnitude of change will be determined by the fluid-rock ratio, the $\delta^{18}O$ value of the meteoric water, and the temperature of alteration. Vital effects can be identified by the deviation from expected equilibrium value (green and orange arrow). Dehydroxylation of bicarbonate during carbonate formation would cause the triple oxygen isotope value to plot somewhere along the green arrow. Hydroxylation of bicarbonate during carbonate formation would cause the triple oxygen isotope value of the precipitating carbonate to plot somewhere along the orange arrow. Note the magnitude and azimuth would change slightly depending on precipitating conditions such as pH, temperature, time, etc. See Guo and Zhou (2019) for more information on the (de)hydroxylation effects.

Figure 5: Calculated $\delta^{18}O$ values of formation waters and corresponding temperatures from carbonate clumped measurements. Temperatures and calculated $\delta^{18}O_{seawater}$ values for the sparry infill (squares) overlap with those of the fossil carbonate (circles and diamond). Red dashed line represents a $\delta^{18}O_{seawater}$ value of -1‰. Most fossil carbonate samples have Δ_{47} values that correspond to calculated $\delta^{18}O_{seawater}$ values that are higher than the canonical -1‰ that represents the global average greenhouse open ocean.

Figure 6: The $\Delta'^{17}O$ and Δ_{47} values from WIS samples. The black curved line represents equilibrium for both systems with an ocean water $\Delta'^{17}O$ -4 ppm. The $\Delta'^{17}O$-Δ_{47} equilibrium line

helps visualize when a sample has preserved primary precipitation temperature or has been altered.

Figure 7: Optimized parameters for alteration temperature (A), alteration fluid $\delta^{18}O$ value (B), and formation temperature (C) after 1000 iterations of the PSO function using all samples from the dataset.

Figure 8: Optimized parameters for alteration temperature (A, D, G, and J), alteration fluid $\delta^{18}O$ value (B, E, H, and K), and formation temperature (C, F, I and L) after 1000 iterations of the PSO function. The samples were separated into four categories: High temperature samples from the Campanian (A, B, C), Low temperature samples from the Campanian (D, E, F), High temperature samples from the Maastrichtian (G, H, I) and Low temperature samples from the Maastrichtian (J, K, L). See main text for explanation of how samples were sorted into groups.

Figure 9: Comparison of triple oxygen isotope temperature and $\delta^{18}O_{seawater}$ results from this study to previous clumped isotope temperatures and $\delta^{18}O_{seawater}$ values from the WIS. Shaded areas represent range of published values, not including reported error. A) Temperatures between 20 and 40°C for the late Campanian (75 to 72 Ma) WIS from this study (green) are within the range of previous studies Gao et al. (2021, blue) and Dennis et al. (2013, purple) but warmer than that reported in Petersen et al. (2016, grey). The early Maastrichtian (69-67 Ma) temperature of 32°C from this study are warmer than those reported in Dennis et al. (2013) and Petersen et al. (2016). Only one Maastrichtian sample from our dataset is pristine. B) This study reports $\delta^{18}O$ values between -3 and 0‰ and agrees with other reported $\delta^{18}O$ values. However, this study suggests that carbonate clumped isotope measurements with calculated $\delta^{18}O$ values of water that are less than -3‰ are an artifact of diagenesis and have reset carbonate clumped isotope values. Note that Petersen et al. (2016) was corrected to the new calibration presented in Jones et al. (2022).

[1]Supplemental Material. Supplementary figures and discussion are provided. Please visit https://doi.org/10.1130/XXXX to access the supplemental material, and contact editing@geosociety.org with any questions.

Figure 1

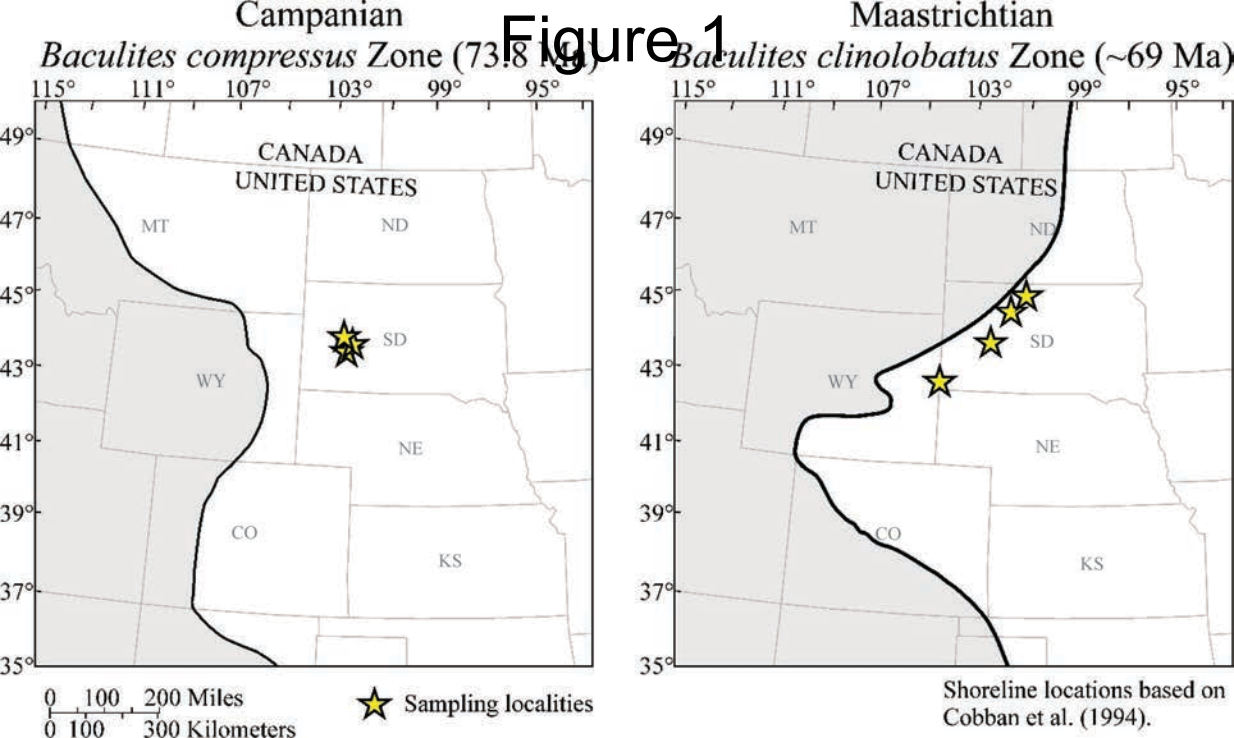
Campanian
Baculites compressus Zone (73.8 Ma)
Maastrichtian
Baculites clinolobatus Zone (~69 Ma)
115°
111°
107°
103°
99°
95°
49°
47°
45°
43°
41°
39°
37°
35°
CANADA
UNITED STATES
MT
ND
SD
WY
NE
CO
KS
0 100 200 Miles
0 100 300 Kilometers
Sampling localities
Shoreline locations based on Cobban et al. (1994).

Figure 2

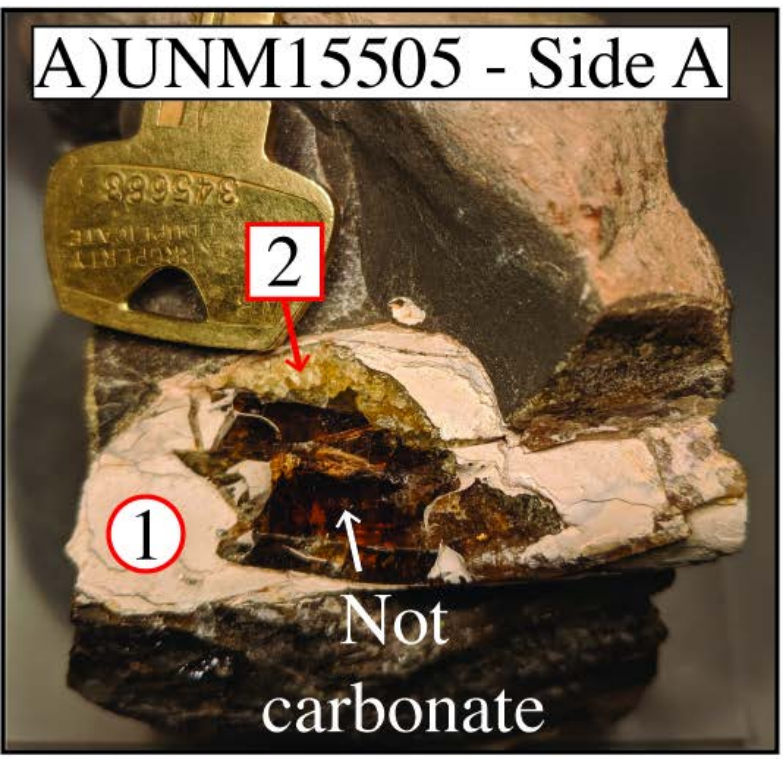
A)UNM15505 - Side A
2
1
Not
carbonate

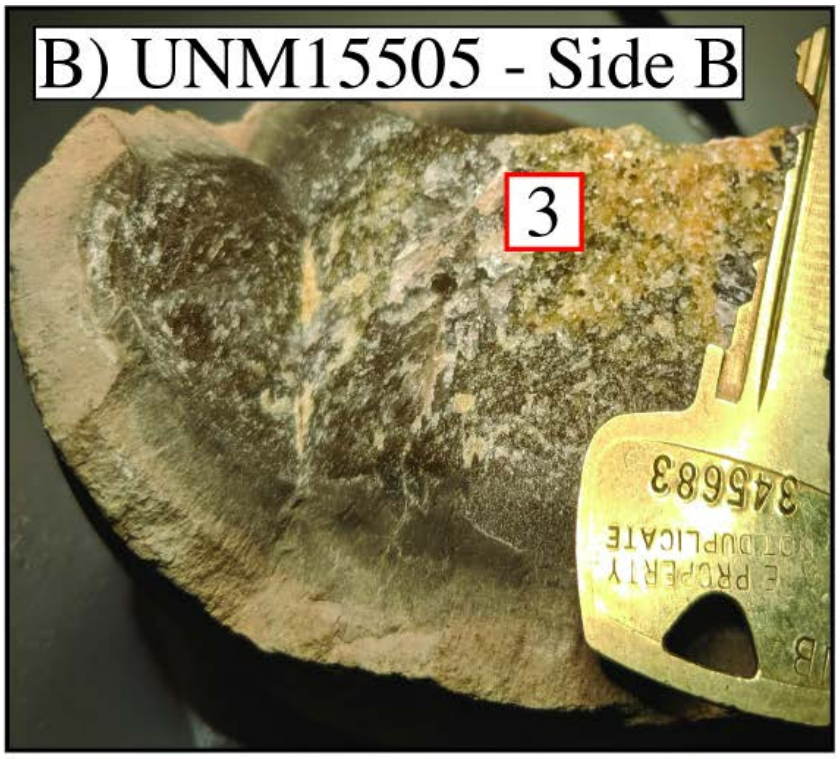
B) UNM15505 - Side B
3

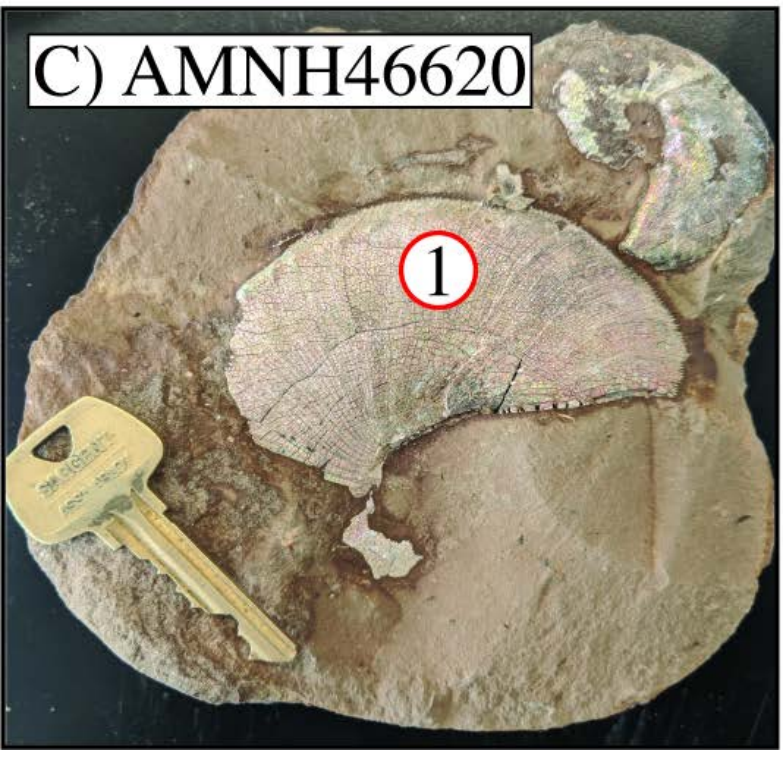
C) AMNH46620
1


D) UNM15504
SARGENT
ASSA ABLOY
1

Figure 3

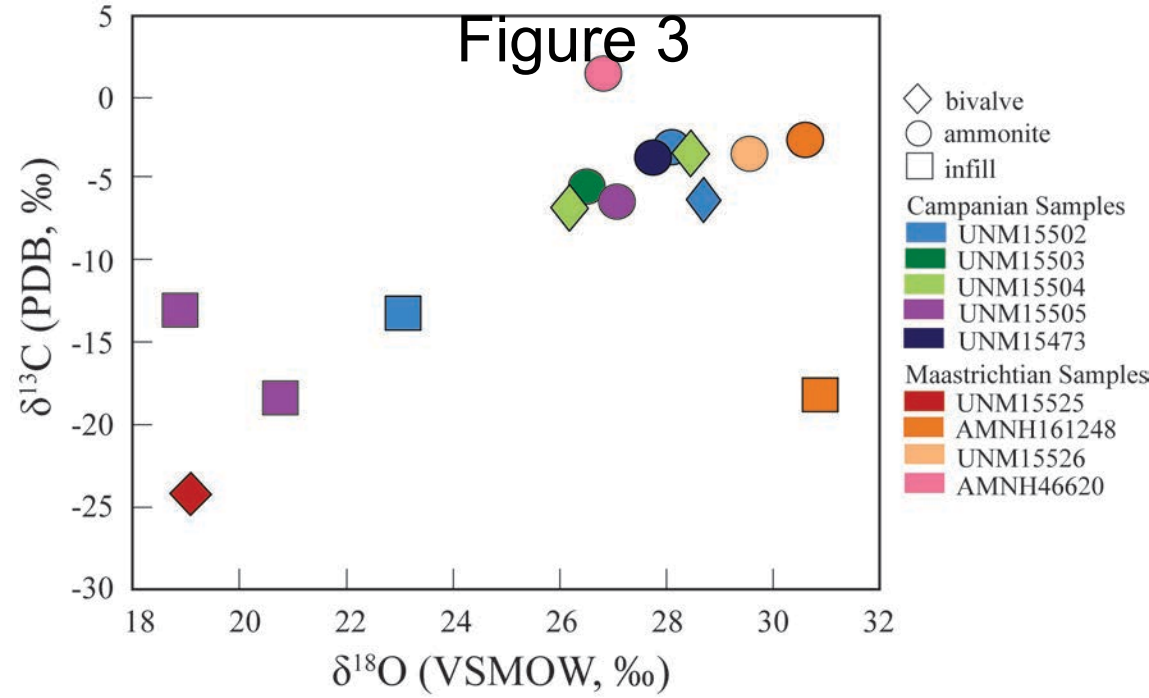
5
0
-5
-10
-15
-20
-25
-30
18
20
22
24
26
28
30
32
δ13C (PDB, ‰)
δ18O (VSMOW, ‰)
bivalve
ammonite
infill
Campanian Samples
UNM15502
UNM15503
UNM15504
UNM15505
UNM15473
Maastrichtian Samples
UNM15525
AMNH161248
UNM15526
AMNH46620

Figure 4

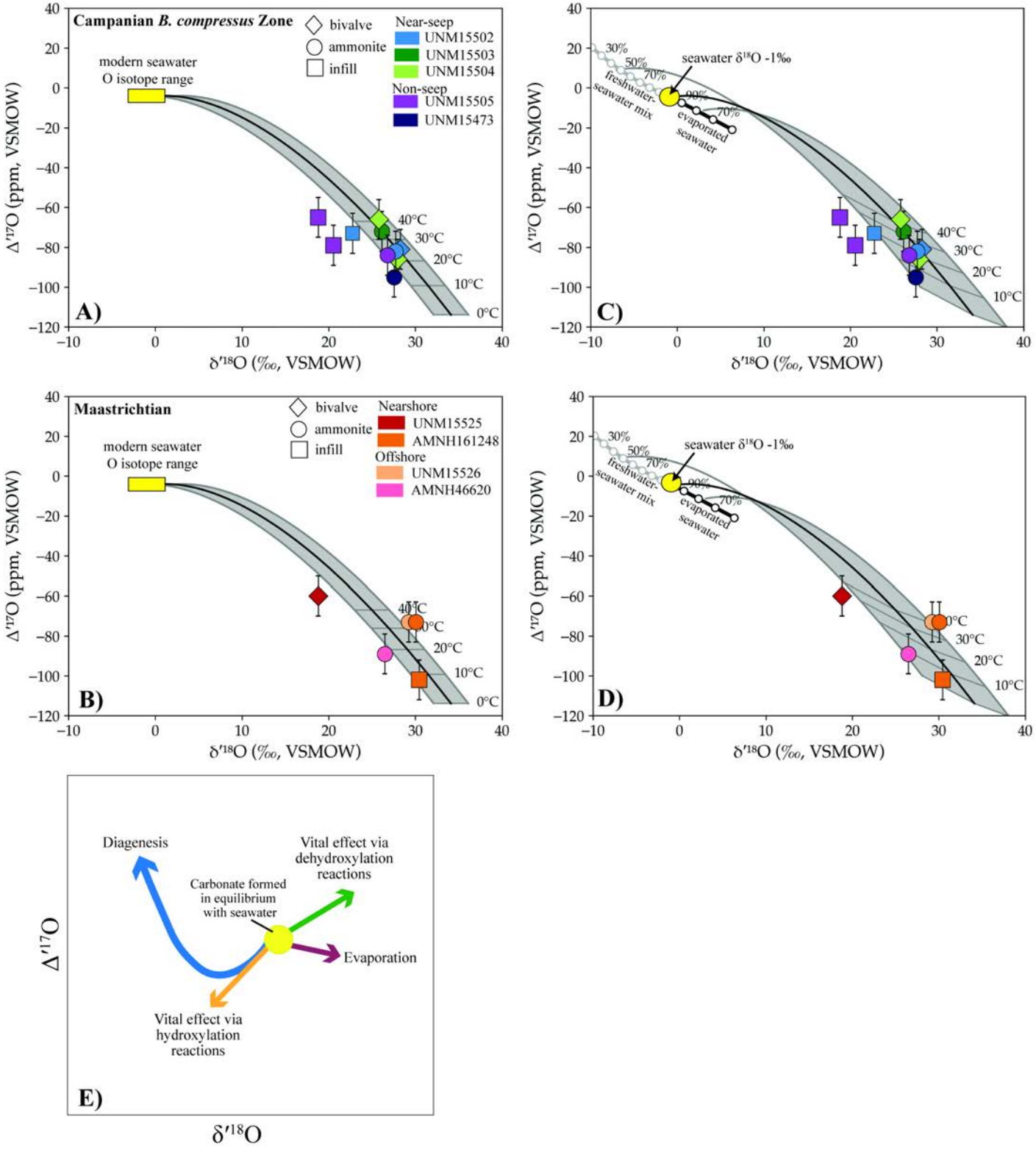
Campanian B. compressus Zone
bivalve
ammonite
infill
Near-seep
UNM15502
UNM15503
UNM15504
Non-seep
UNM15505
UNM15473
modern seawater
O isotope range
40°C
30°C
20°C
10°C
0°C
A)
Δ′17O (ppm, VSMOW)
δ′18O (‰, VSMOW)
seawater δ18O -1‰
30%
50%
70%
90%
freshwater-
seawater mix
evaporated
seawater
C)
Maastrichtian
Nearshore
UNM15525
AMNH161248
Offshore
UNM15526
AMNH46620
B)
D)
Diagenesis
Vital effect via
dehydroxylation
reactions
Carbonate formed
in equilibrium
with seawater
Evaporation
Vital effect via
hydroxylation
reactions
E)
Δ′17O
δ′18O

Figure 5

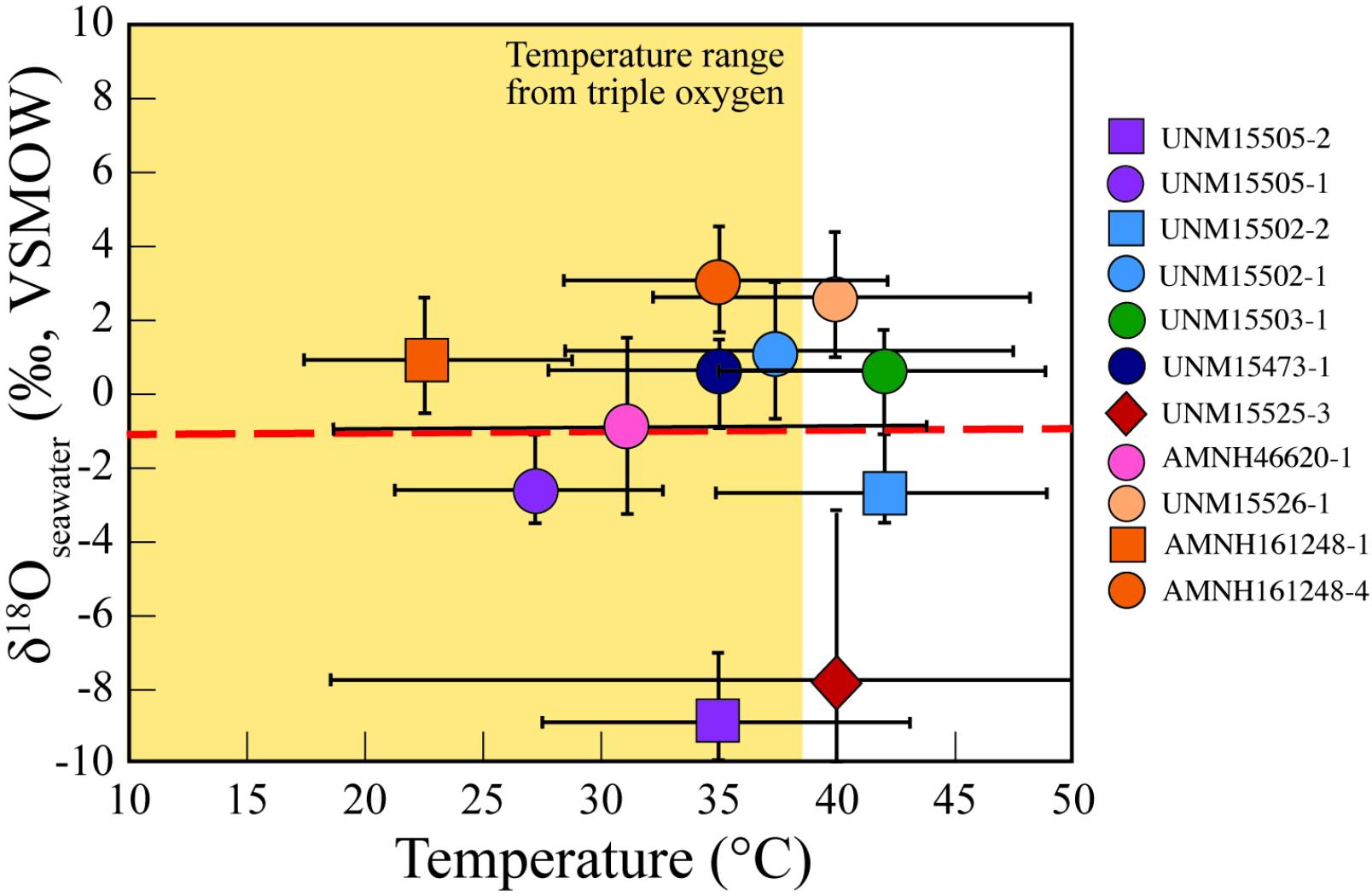
Temperature range
from triple oxygen
10
8
6
4
2
0
-2
-4
-6
-8
-10
10
15
20
25
30
35
40
45
50
δ18Oseawater (‰, VSMOW)
Temperature (°C)
UNM15505-2
UNM15505-1
UNM15502-2
UNM15502-1
UNM15503-1
UNM15473-1
UNM15525-3
AMNH46620-1
UNM15526-1
AMNH161248-1
AMNH161248-4

Figure 6

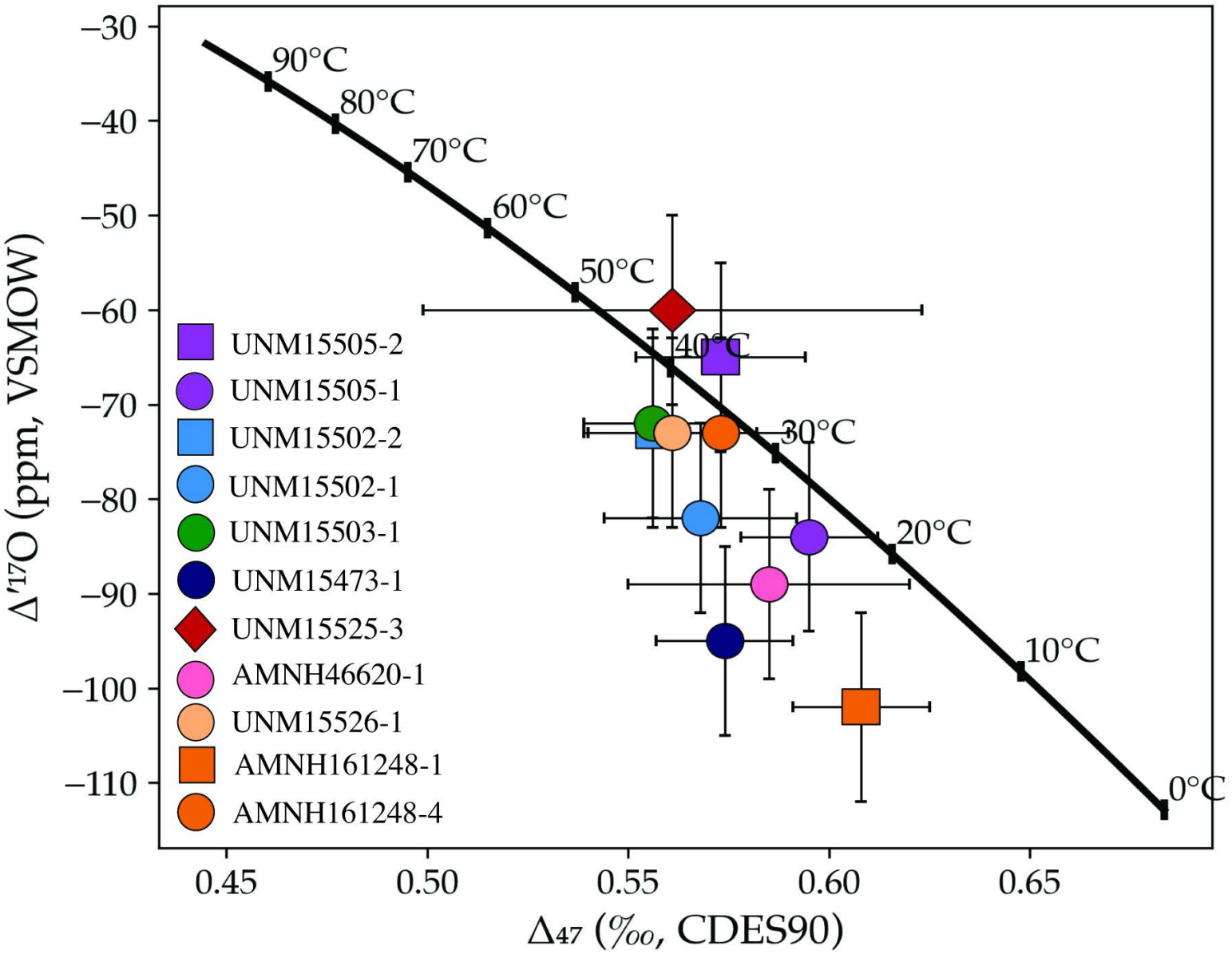
−30
−40
−50
−60
−70
−80
−90
−100
−110
Δ'17O (ppm, VSMOW)
0.45
0.50
0.55
0.60
0.65
Δ47 (‰, CDES90)
90°C
80°C
70°C
60°C
50°C
40°C
30°C
20°C
10°C
0°C
UNM15505-2
UNM15505-1
UNM15502-2
UNM15502-1
UNM15503-1
UNM15473-1
UNM15525-3
AMNH46620-1
UNM15526-1
AMNH161248-1
AMNH161248-4

Figure 7

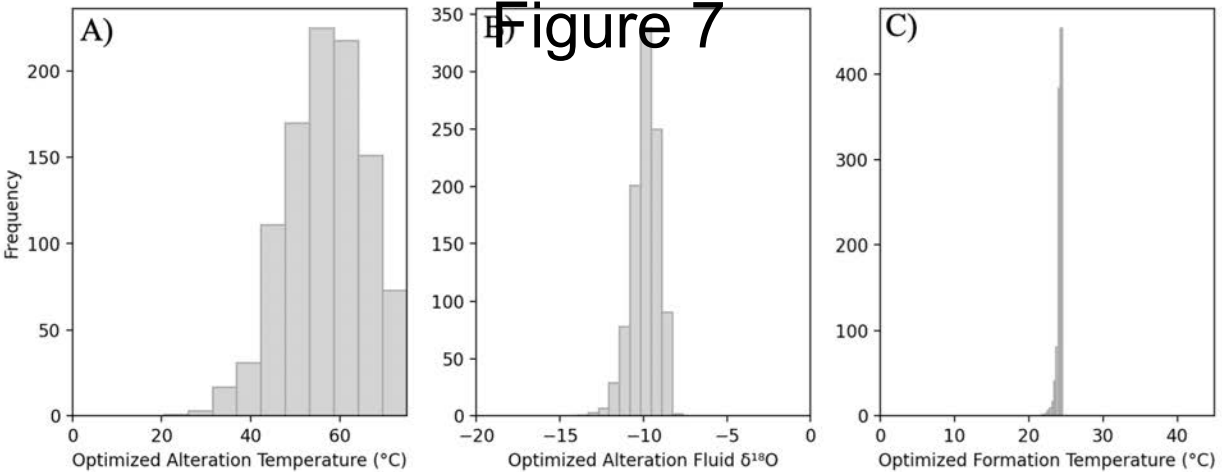
A)
B)
C)
Frequency
Optimized Alteration Temperature (°C)
Optimized Alteration Fluid δ18O
Optimized Formation Temperature (°C)

Figure 8

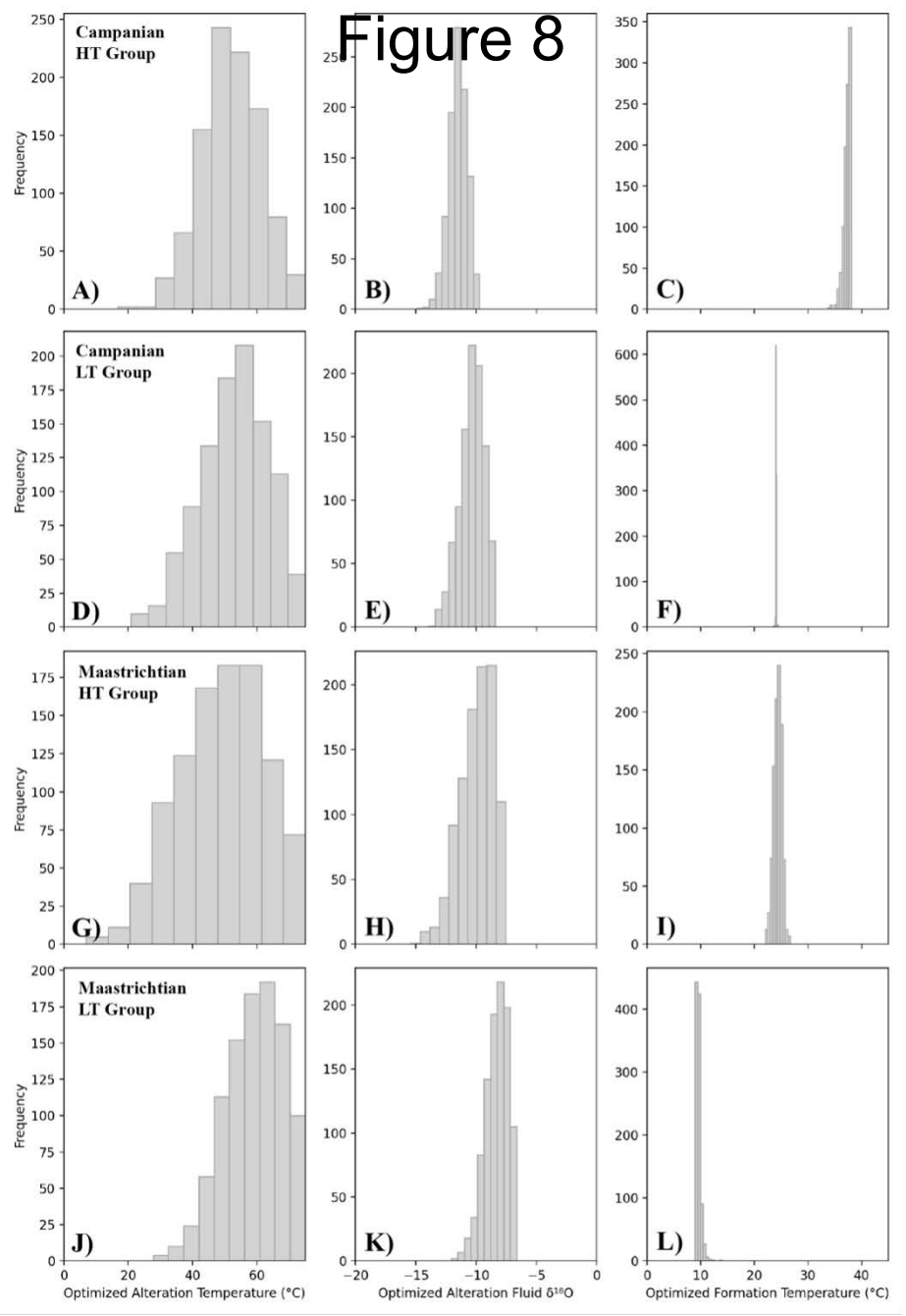
Campanian
HT Group
A)
B)
C)
Campanian
LT Group
D)
E)
F)
Maastrichtian
HT Group
G)
H)
I)
Maastrichtian
LT Group
J)
K)
L)
Frequency
Optimized Alteration Temperature (°C)
Optimized Alteration Fluid δ18O
Optimized Formation Temperature (°C)

Figure 9

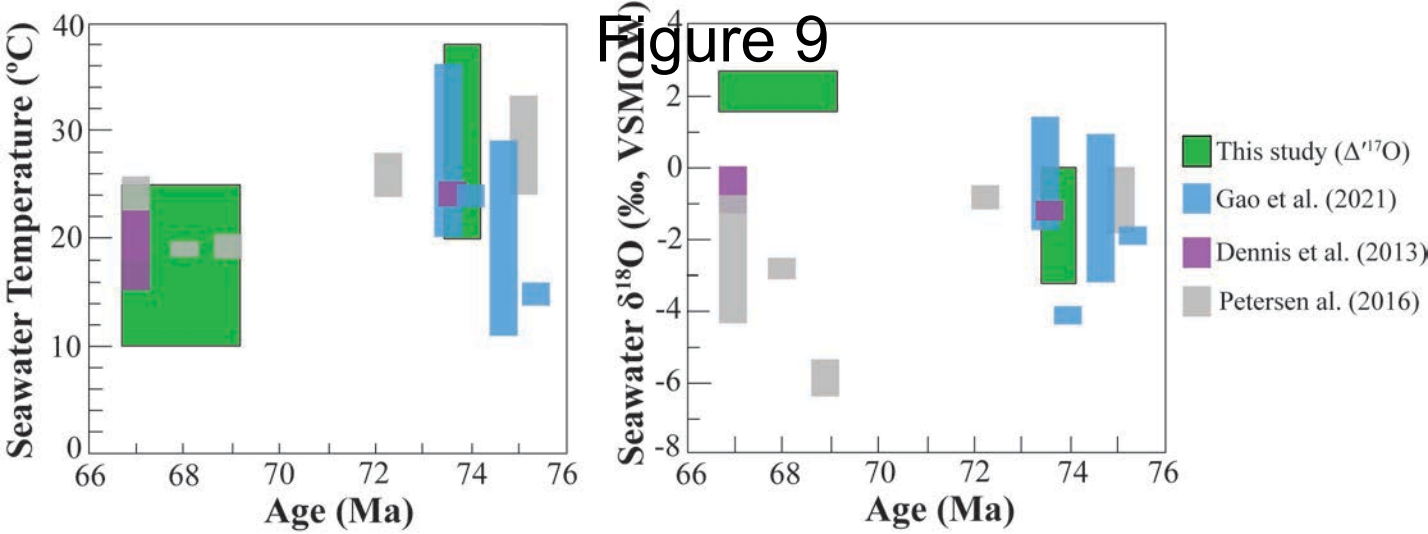
Seawater Temperature (°C)
40
30
20
10
0
66
68
70
72
74
76
Age (Ma)
Seawater δ18O (‰, VSMOW)
4
2
0
-2
-4
-6
-8
66
68
70
72
74
76
Age (Ma)
This study (Δ'17O)
Gao et al. (2021)
Dennis et al. (2013)
Petersen al. (2016)

Table 1: Sample information for concretions used in this study.

Sample ID	Type	Age (Ma)	Taxon	Biozone	Stratigraphy	Locale	Lat/Long	Locale #	Habitat*
UNM15502-1	Shell	73.8	*Hoploscaphites* sp.	*B. compressus*	Pierre Shale Fm	Patterson Ranch, SD	44.17306 N -102.40194 W	AMNH 3528	O/S
UNM15502-2	Infill	73.8	N/A	*B. compressus*	Pierre Shale Fm	Patterson Ranch, SD	44.17306 N -102.40194 W	AMNH 3528	O/S
UNM15502-4	Shell	73.8	Inoceramid bivalve	*B. compressus*	Pierre Shale Fm	Patterson Ranch, SD	44.17306 N -102.40194 W	AMNH 3528	O/S
UNM15503-1	Shell	73.8	*Placenticeras meeki*	*B. compressus*	Pierre Shale Fm	Patterson Ranch, SD	44.17306 N -102.40194 W	AMNH 3528	O/S
UNM15504-1	Shell	73.8	*Nymphalucina occidentalis*	*B. compressus*	Pierre Shale Fm	Patterson Ranch, SD	44.17306 N -102.40194 W	AMNH 3528	O/S
UNM15504-2	Shell	73.8	Inoceramid bivalve	*B. compressus*	Pierre Shale Fm	Patterson Ranch, SD	44.17306 N -102.40194 W	AMNH 3528	O/S
UNM15473-1	Shell	73.8	*Baculites compressus*	*B. compressus*	Pierre Shale Fm	Trask Ranch, SD	44.1359 N -102.2412 W	AMNH 3966	O/NS
UNM15505-1	Shell	73.8	*Baculites compressus*	*B. compressus*	Pierre Shale Fm	Smith Ranch, SD	44.2375 N -102.5761 W	UNM 1706A	O/NS
UNM15505-2	Infill	73.8	N/A	*B. compressus*	Pierre Shale Fm	Smith Ranch, SD	44.2375 N -102.5761 W	UNM 1706A	O/NS
UNM15505-3	Infill	73.8	N/A	*B. compressus*	Pierre Shale Fm	Smith Ranch, SD	44.2375 N -102.5761 W	UNM 1706A	O/NS
UNM15526-1	Shell	69	*Hoploscaphites melloi*	*H. birklundae*	Pierre Shale Fm	White Ranch, SD	44.401487 N -102.102057 W	AMNH 3294	O/NS
UNM15525-3	Shell	69	Unknown bivalve	*H. birklundae*	Fox Hills Fm	Red Bird, WY	43.31998 N -104.25912 W	AMNH 3589	N/NS
AMNH46620-1	Shell	68	*Hoploscaphites nicolletii*	*H. nicolletii*	Pierre Shale Fm (Elk Butte Mbr)	Moreau River, SD	45.213317 N -101.512167 W	AMNH 3302	O/NS
AMNH161248-4	Shell	67	*Hoploscaphites* sp.	*H. nebrascensis*	Fox Hills Fm (Timber Lake Mbr)	Corson and Dewey Counties, SD	45.43483 N -101.35 W	AMNH 3272	N/NS
AMNH161248-1	Infill	67	N/A	*H. nebrascensis*	Fox Hills Fm (Timber Lake Mbr)	Corson and Dewey Counties, SD	45.43483 N -101.35 W	AMNH 3272	N/NS

* Offshore (O) or Nearshore (N)/Seep (S) or Non-Seep (NS)

Table 2: Chemical composition, expressed as %, of fossil carbonate samples based on XRD results.

Sample ID	Calcite	Aragonite	Quartz	Amorphous/Others
UNM15502-1	6.2	71.8		22.0
UNM15503-1		100		
UNM15473-1	12.4	87.6		
UNM15505-1	32.2	67.8		
UNM15526-1	11.1	88.9		
UNM15525-3	82.7	13.9	3.3	
AMNH46620-1		100		
AMNH161248-4	10.0	90.0		

Table 3: Carbonate clumped (Δ_{47}) isotope values, along with $\delta^{13}C$ and $\delta^{18}O$, of Cretaceous fossil shells and calcite infill, measured at Stony Brook University. T(Δ_{47}) is calculated using the calibration of Petersen et al. (2019). The calculated $\delta^{18}O$ value of the water is calculated by using the T(Δ_{47}) and measured carbonate $\delta^{18}O$ using the carbonate-water oxygen isotope equation of Wostbrock et al. (2020a), suitable to use for both aragonite-water and for calcite-water. Error is reported as the 95% confidence interval. Average standard deviation for the $\delta^{13}C$ and $\delta^{18}O$ values is 0.15 and 0.14 ‰, respectively.

Sample ID	Type	Carb Type	Age (Ma)	n	$\delta^{13}C$ (‰, VPDB)	$\delta^{18}O_{carb}$ (‰, VSMOW)	Δ_{47} (‰)	Δ_{47} Error (‰)	T(Δ_{47}) (°C)	T(Δ_{47}) Error (°C)	$\delta^{18}O_{water}$ (‰, VSMOW)	$\delta^{18}O_{water}$ Error (‰)
UNM15502-1	Shell	Arg	73.8	2	-3.5	28.27	0.568	0.024	37	10	1.3	1.8
UNM15502-2	Infill	Cal	73.8	3	-13.2	23.66	0.560	0.017	42	7	-2.3	1.3
UNM15503-1	Shell	Arg	73.8	3	-5.0	26.66	0.556	0.017	42	7	0.6	1.3
UNM15473-1	Shell	Arg	73.8	3	-4.1	27.91	0.574	0.017	35	6	0.5	1.2
UNM15505-1	Shell	Arg	73.8	3	-6.8	26.40	0.595	0.017	27	6	-2.5	1.2
UNM15505-2	Infill	Cal	73.8	3	-13.3	18.15	0.573	0.021	35	8	-9.0	1.3
UNM15526-1	Shell	Arg	69	2	-10.8	29.08	0.561	0.021	40	8	2.6	1.5
UNM15525-3	Shell	Arg	69	2	-24.5	18.27	0.561	0.062	40	25	-7.9	4.6
AMNH46620-1	Shell	Arg	68	2	1.8	27.34	0.585	0.035	31	13	-0.9	2.5
AMNH161248-4	Shell	Arg	67	3	-2.4	30.56	0.573	0.017	35	6	3.1	1.2
AMNH161248-1	Infill	Cal	67	3	-18.2	31.06	0.608	0.017	23	6	1.0	1.2

Table 4: Carbonate $\delta^{13}C$, $\delta^{17}O$, $\delta^{18}O$, and $\Delta'^{17}O$ values of Cretaceous fossil shells and calcite infill, measured at the University of New Mexico. All isotope values are reported in ‰ and relative to VSMOW, unless indicated. Based on XRD data, all shells are assumed to be mostly aragonite (Arg) and infill calcite (Cal). $T(\Delta'^{17}O)$ and $\delta^{18}O_{water}$ values are calculated for samples that plot within the equilibrium field using equations from Wostbrock et al. (2020a). Samples without temperature or water $\delta^{18}O$ calculations have been altered and no longer contain primary precipitation values, although results of a fluid-rock mixing model suggest an initial precipitation temperature of ~25°C. Note, $\delta^{17}O$ and $\delta^{18}O$ values are reported to the third decimal place for calculation of the $\Delta'^{17}O$ values ($\delta^{18}O$ and $\delta^{17}O$ covary, leading to the high $\Delta'^{17}O$ precision). Average standard deviations for the $\delta^{13}C$, $\Delta'^{17}O$, and $\delta^{18}O$ values are 0.23 ‰, 10ppm, and 0.18 ‰, respectively.

Sample ID	Type	Carb Type	Age (Ma)	$\delta^{13}C$ (VPDB)	$\delta^{17}O_{carb}$	$\delta^{18}O_{carb}$	$\Delta'^{17}O$	$T(\Delta'^{17}O)$ (±10°C)	$\delta^{18}O_{water}$ (±2‰)
UNM15502-1	Shell	Arg	73.8	-3.3	14.646	28.083	-82	23	-1.6
UNM15502-2	Infill	Cal	73.8	-13.6	12.020	23.028	-73		
UNM15502-4	Shell	Arg	73.8	-6.6	14.954	28.670	-81	24	-0.9
UNM15503-1	Shell	Arg	73.8	-5.4	13.823	26.475	-72	33	-1.1
UNM15504-1	Shell	Arg	73.8	-6.4	13.646	26.133	-66	41	-0.3
UNM15504-2	Shell	Arg	73.8	-3.8	14.757	28.303	-86	20	-2.2
UNM15473-1	Shell	Arg	73.8	-3.9	14.549	27.917	-95		
UNM15505-1	Shell	Arg	73.8	-6.1	14.149	27.130	-84	22	-3.0
UNM15505-2	Infill	Cal	73.8	-13.2	9.905	18.965	-65		
UNM15505-3	Infill	Cal	73.8	-18.2	10.840	20.775	-79		
UNM15526-1	Shell	Arg	69	-3.7	15.483	29.672	-73	32	1.7
UNM15525-3	Shell	Arg	69	-24.4	9.916	18.982	-60		
AMNH46620-1	Shell	Arg	68	1.9	13.982	26.822	-89		
AMNH161248-4	Shell	Arg	67	-2.4	15.921	30.520	-73	32	2.8
AMNH161248-1	Infill	Cal	67	-18.3	15.961	30.892	-102		